1
Anatomic, Physiologic and Metabolic Imaging in Neuro-Oncology

Sanjeev Chawla, Harish Poptani, and Elias R. Melhem

1 Introduction

Primary brain tumors arise from various cell types of the brain, including glial cells, neurons, neuroglial precursor cells, pinealocytes, pericytes of the vessels, cells of the hypophysis, lymphocytes and the meninges [1, 2]. The incidence of primary brain tumors varies between subtypes, with the most common primary brain tumors in adults being gliomas and meningiomas.

Gliomas can be histologically classified into astrocytomas, oligodendrogliomas, mixed oligoastrocytomas, ependymal tumors and tumors of the choroid plexus. Tumor malignancy or grade is generally assessed according to the World Health Organization (WHO) criteria, taking into account the presence of nuclear changes, mitotic activity, endothelial proliferation and necrosis [1, 3]. The most fatal and common primary brain neoplasm is the glioblastoma multiforme (GBM), which corresponds to WHO grade IV. Despite aggressive multimodal treatment strategy (surgery, radiation and chemotherapy), median survival of patients with GBM is limited to less than 14 months. A complex series of molecular events occur during tumor growth resulting in dysregulation of the cell cycle, alterations in apoptosis and cell differentiation, neo-vascularization as well as tumor cell migration and invasion into the normal brain parenchyma. Genetic alterations also play an important role in the development of glioma, including a loss, mutation or hypermethylation of the tumor suppressor gene, such as p53 or other genes involved in the regulation of the cell cycle. During progression from low-grade to high-grade, step-wise accumulation of genetic alterations occurs. Growth of certain tumors seems to be related to the presence of viruses and familial diseases that accelerate the progression of molecular alterations, or exposure to environmental chemicals, pesticides, herbicides and fertilizers [4-6].

A better understanding of tumorgenesis is crucial for the development of specific molecular therapies that specifically target the tumor and reduce patient morbidity and mortality. Positron emission tomography (PET), computed tomography (CT) and magnetic resonance imaging (MRI) are generally used for non-invasive diagnosis and

Department of Radiology, University of Pennsylvania, Philadelphia, Pennsylvania, United States

M.A. Blake and M.K. Kalra (eds.), *Imaging in Oncology.*

understanding of tumor growth mechanism. Cranial CT and MRI, with and without contrast media, are widely used for primary diagnosis of brain tumors. CT is used for detection of calcifications in oligodendrogliomas, meningiomas or craniopharyngiomas, and for tumors that are located at the base of the skull. However, the discrimination of tumor boundaries from normal tissue or vasogenic edema, as well as the evaluation of tissue heterogeneity and tumor grading are often a challenge and are not adequately reflected on CT. Furthermore, the use of ionizing radiation and image acquisition only in the axial plane, limits its applicability.

PET uses various radioactive agents to detect differences in metabolic and chemical activity in the body. PET measures a wide range of physiologic processes critical in understanding the pathophysiology of brain tumors with high sensitivity. It allows for detection of metabolic changes that occur prior to structural changes visible on CT and conventional MR images. However, the major limitation of PET is its relatively poor spatial resolution and a high incidence of false positives.

Continuous developments in MRI provide new insights into the diagnosis, classification and understanding of the biology of brain tumors. MRI offers several advantages compared to CT and PET. MRI offers excellent spatial resolution ($1 \times 1 \times 1\,mm^3$ in humans), very high gray-white matter contrast and acquisition of multiplanar images. MRI is particularly accurate in establishing the intra- or extra-axial origin of tumors. The use of three-dimensional (3-D) image acquisition and reconstruction with MRI is not only limited to diagnosis, but is also useful for pre-surgical planning, stereotactic procedures and radiotherapy. Despite optimization of sequences and protocols, the classification and grading of gliomas with conventional MRI is sometimes unreliable, with the sensitivity for glioma grading ranging from 55.1 percent to 83.3 percent [7]. Integration of diagnostic information from advanced MRI techniques like proton magnetic resonance spectroscopy (^{1}H MRS), diffusion and perfusion-weighted imaging and functional MRI (fMRI) can further improve the classification accuracy of conventional anatomical MRI [8]. Advanced MRI techniques are also being used to gain additional information on metabolic and molecular tumor markers [9, 10]. In selected patients, MRI and PET are being used in conjunction to define the real extent of the tumor [11].

2 Magnetic Resonance Imaging

2.1 Diagnosis and Grading of Brain Tumors

2.1.1 Conventional MRI

General Features of Brain Tumors

Due to the excellent soft tissue contrast and high spatial resolution, MRI provides exquisite anatomical details that aid in diagnosis, classification and understanding the biology of brain tumors. A routine MRI examination of patients with brain

tumors includes long TR/long TE (T2-weighted), short TR/short TE (T1-weighted), fluid-attenuated inversion recovery (FLAIR) and post-contrast T1 sequences. Detection of a tumor is based primarily on the presence of mass effect and signal alteration on these imaging sequences. The three main variables that differentiate tumors from normal tissue are: water content, regressive events and vascular architecture. Most brain tumors exhibit increased water content and, thus, appear hyperintense on T2-weighted and FLAIR images, and hypointense on T1-weighted images (Fig. 1.1 a,b, c and Fig. 1.2a,b, c). This hyperintensity is more pronounced in masses having a low nucleus/cytoplasm ratio (e.g., astrocytoma), than in masses with a high nucleus/cytoplasm ratio (e.g., medulloblastoma). The peritumoral hyperintensity on T2-weighted images is generally nonspecific and is thought to be due to tumor infiltration, vasogenic edema, or both.

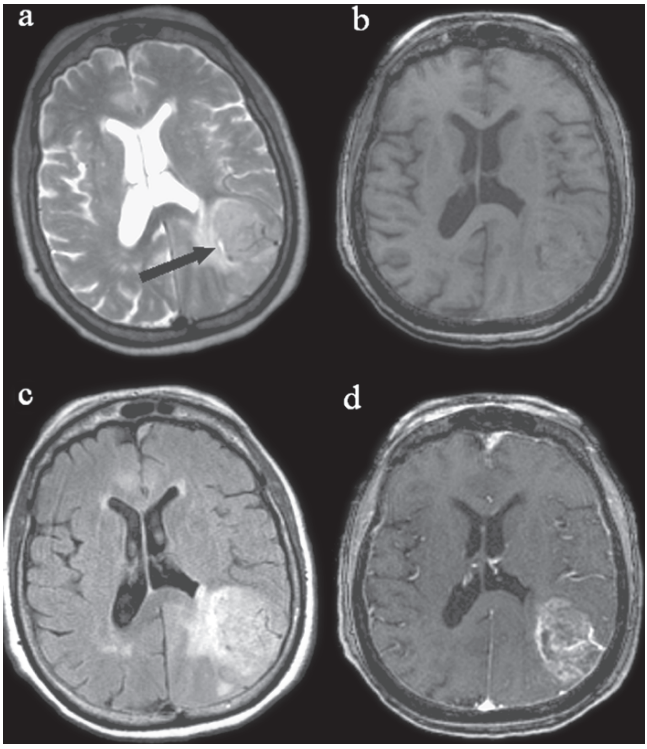

Fig. 1.1 High-grade glioma. Axial T2-weighted image (**a**) demonstrates an ill-defined, hyperintense (compared to gray matter), heterogeneous mass in the left parietal lobe along with vasogenic edema along the white matter tracts. Note the presence of necrotic foci (arrow) within the tumor. This mass appears as iso to hypointense on T1-weighted image (**b**) and hyperintense on FLAIR image (**c**). There is a heterogeneous contrast enhancement within the mass on the corresponding post contrast T1-weighted image (**d**)

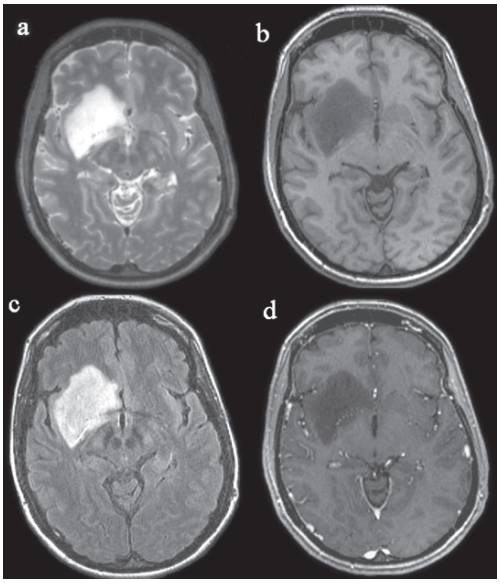

Fig. 1.2 Low-grade glioma. Axial T2-weighted image (**a**) demonstrates a homogenously hyperintense mass in the insular region extending into the right frontal lobe. This mass is well circumscribed with minimal mass effect and edema that appears hypointense on T1-weighted image (**b**) and hyperintense on FLAIR image (**c**). There is no evidence of abnormal contrast enhancement on the post contrast T1-weighted image (**d**)

Regressive events such as cyst formation, necrosis and hemorrhage, calcifications and fatty degenerative areas modulate the MRI appearance of brain tumors. Intratumoral cysts are secondary to focal mucoid degeneration and fluid transudation from cyst walls. Cysts can be filled with water, or contain considerable amounts of protein or other debris from prior hemorrhage. If the cyst contains water only, it has the same signal intensity as cerebrospinal fluid (CSF) on T2- and T1-weighted images. When the protein content increases, protons become bound in a hydration layer adjacent to the protein, significantly decreasing the T1 relaxation time of water, leading to an increase in the signal intensity on FLAIR and T1-weighted images. Necrotic areas result from ischaemic cell damage or intratumoral hemorrhagic events that result in the formation of pseudocystic areas. These areas typically appear hyperintense on T2 and hypointense on T1-weighted images, compared to normal brain parenchyma.

Certain primary intracranial neoplasms and metastatic tumors demonstrate hemorrhage and calcification [12]. Both chronic hemorrhage and calcifications appear hypointense on T2 and T2-weighted images, due to the induction of paramagnetic susceptibilities [13]. Recently, corrected gradient echo phase imaging has been used to differentiate hemorrhage and calcification [14, 15]. An abnormal vascular architecture is a feature that is generally observed in tumors. Stimulation of the formation of new capillaries (neo-vasculature) within the tumor tissue is facilitated

by hypoxia and endothelial growth factor receptors (EGFR). In malignant gliomas, formation of capillaries with fenestrated endothelia is stimulated, which leads to disruption of the blood-brain barrier (BBB) and contrast enhancement [16], as shown on Fig. 1-1d. On the other hand, in some tumors with a functioning BBB, these capillaries exhibit near-normal features, hence, these tumors do not enhance on contrast-enhanced T1-weighted images [16] as shown on Fig. 1.2d.

Metastatic tumors are characterized by the presence of typically leaky, non-central nervous system capillaries similar to their tissue of origin and, hence, exhibit intense enhancement. Extra-axial tumors, like meningiomas, arise from tissue whose capillaries lack tight junctions and, consequently, these tumors also exhibit contrast enhancement [16]. While the extent of a tumor in the brain can be evaluated by contrast enhancement, it is known that invasive tumor cells are also present beyond the enhancing portion of the tumor, particularly in gliomas. Since contrast enhancement on conventional MRI indicates disruption of BBB and not underlying regional vascularity, it cannot be used to predict histological grade [17]. However, Fayed, et al. [18] have reported a significant difference in the contrast-to-noise ratio (CNR) of gadolinium-enhancement between low- and high-grade gliomas. Using a CNR threshold of 35.86, these authors reported a sensitivity of 82.6 percent and a specificity of 91.7 percent for the prediction of malignancy.

Besides primary information on the size and location of the tumor, conventional MRI (T1, T2 and post-contrast T1 images) provides additional information about secondary phenomena such as mass effect, edema, hemorrhage, necrosis and signs of increased intracranial pressure.

General Features that Differentiate Intra-axial from Extra-axial Tumors

Differentiation between intra-axial and extra-axial masses is crucial as clinical management of these tumors is different [19]. This distinction has been made easier by multiplanar capabilities of MRI. Key features that help in identifying an intra-axial mass include gyral expansion, thinning or effacement of the adjacent extra-axial subarachnoid space and peripheral displacement of blood vessels along the pial surface of the brain (best seen on contrast-enhanced images) [19]. Imaging features more characteristic of extra-axial intradural masses include local bony changes such as hyperostosis, or widening of pre-existing foramina or canals; displacement of brain surface vessels away from bone and dura; white matter buckling, and widening of the subarachnoid space adjacent to the mass; central displacement of both the gray-white junction and presence of blood vessels along the pial surface. Extradural masses show similar behavior, but they usually displace the dural sheet centrally [19].

Common Brain Tumors Occurring in Adults

Intra-axial Tumors

The most common tumors of intra-axial location are gliomas and metastases. Gliomas derived from brain cells can, thus, be classified as true brain tumors,

whereas metastases are deposits from extradural malignancies. Gliomas tend to be poorly demarcated from the normal brain parenchyma, whereas metastases are generally demarcated sharply. In cerebral hemispheric masses, imaging in the axial or coronal plane is usually best, whereas for lesions at or near the midline, sagittal imaging is often most informative. Typically, low-grade astrocytomas demonstrate increased signal intensity on T2-weighted images and are well circumscribed with no evidence of hemorrhage or necrosis [20]. On the other hand, GBMs – the most aggressive of the gliomas – are characterized by the presence of necrosis within the tumor, coupled with extensive peritumor finger-like edema along the white matter tracts. Oligodendrogliomas may preferentially involve the cortical gray matter and foci of cystic degeneration are relatively common [12]. Many imaging characteristics of oligodendroglioma are similar to those of astrocytomas. Gyriform or ribbon-like pattern of calcification is frequently seen in oligodendrogliomas. It has been reported that FLAIR images tend to be superior to T2-weighted images in rendering greater tumor conspicuity and in depicting margins of oligodendrogliomas [21].

Contrast enhancement is helpful for differential diagnosis, as well as tumor grading. Low-grade fibrillary astrocytomas (WHO grade II) typically do not enhance, whereas anaplastic astrocytomas (grade III) either do not enhance or enhance focally. Pilocytic astrocytomas, though grade I tumors, often enhance markedly, at least in part. High-grade gliomas like GBMs nearly always enhance, however, the degree of enhancement depends on the relative proportions of viable tumor and tumor necrosis [22].

Intracranial metastases account for up to 40 percent of all adult brain neoplasms [23]. Metastases typically involve the cerebral or cerebellar hemispheres at the corti-comedullary junction. These tumors usually appear as relatively well-defined masses in peripheral locations that demonstrate moderate edema and contrast enhancement (Fig. 1.3), however the enhancement of these tumors may be variable, such as solid, ring- like, irregular, homogenous or heterogeneous. Since ring enhancement is frequently observed in brain metastases, a single lesion may be mistaken for a GBM [12]. Contrast-enhanced T1-weighted images are most sensitive in detecting brain metastases, particularly lesions in the posterior fossa or multiple punctate metastases [24]. Some studies have reported that a triple dose of gadolinium is significantly better than a single dose for demonstration of metastases [25, 26]. Metastatic lesions of 1 cm or greater in diameter can be easily detected with a standard dose of contrast while a triple dose of gadolinium is necessary to detect lesions that are smaller than 5 mm in diameter [25]. Recently, it has been reported that the inclusion of FLAIR images along with pre- and post-contrast T1-weighted images aids in differentiating glioma from metastasis in patients with a solitary enhancing lesion, as gliomas frequently exhibit FLAIR signal abnormality in the non-enhancing adjacent cortex of the tumor [27].

Extra-axial Tumors

The most common extra-axial tumors are meningiomas and schwannomas. Meningiomas develop from meningothelial cells while schwannomas arise from

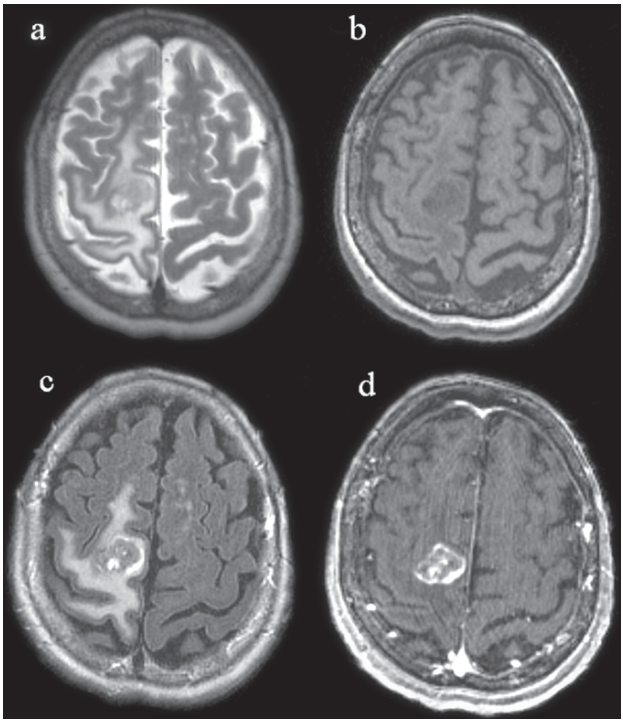

Fig. 1.3 Solitary cerebral metastatic tumor from lung carcinoma. Axial T2-weighted image (**a**) shows a hyperintense mass along with surrounding fingerlike vasogenic edema involving the posterior right frontal lobe that appears hypointense on T1-weighted image (**b**) and hyperintense on FLAIR (**c**). The mass demonstrates partial rim enhancement along with centrally placed enhancing nodules on post-contrast T1-weighted image (**d**)

the nerve sheath, most commonly that of the vestibular portion of the eighth cranial nerve. Meningiomas are typically globular, sometimes lobulated masses attached to the dura that indent the brain and show comparatively little or no edema. Typically meningiomas appear iso- to hyperintense relative to gray matter on T2-weighted images, and iso- to slightly hypointense on T1-weighted images. They exhibit sharp margins, and the enhancement is often intense and homogeneous. At the point of attachment, meningiomas may induce hyperostosis or dural thickening. Abnormal dural enhancement may extend beyond the site of attachment [28, 29].

Schwannomas most commonly occur in the cerebello-pontine (CP) angle cistern, but may also arise from the oculomotor, facial and trigeminal nerves. Schwannomas usually differ from meningiomas in that they typically have a higher signal on T2-weighted images [30].

Less Common Brain Tumors

Intra-axial Tumors

Lymphomas, hemangioblastomas and gliomatosis cerebri are less common intra-axial tumors. Lymphomas most often involve the cerebral hemispheres; typically the white matter and basal ganglia, and approximately half are multifocal. Tumor extension to the ependymal or subarachnoid surfaces is common. The dense packing of tumor cells results in relative hypointensity on T2-weighted images, which is accentuated by the often-pronounced edema. Contrast enhancement is intense and generally solid; ring enhancement, secondary to central necrosis, is more common in immunocompromised than in immunocompetent patients [31].

Hemangioblastomas are highly vascular tumors of the cerebellum that often contain cysts. The MR signal of larger cysts usually differs from that of CSF due to a higher protein content of the cyst fluid. The solid tumor nodule varies in signal intensity, but typically shows strong, intense contrast enhancement. Gliomatosis cerebri is defined as a diffuse neoplastic glial cell infiltration of the brain involving several cerebral lobes. The abnormal cells grow along fiber tracts without destroying the brain parenchyma. Histologically, gliomatosis cerebri varies from grade II to IV, but contrast enhancement is rare. T2-weighted images show widespread hyperintensity of enlarged white matter structures, which cross the borders of lobes, the midline via the corpus callosum, or the level of the tentorium cerebelli [32].

Extra-axial Tumors

Epidermoid cysts are lined by squamous cells and contain cholesterol and keratinized epithelial debris. Common locations of these benign lesions, which slowly expand and distort the CSF spaces, are the midline, the lateral ventricles, and the CP angle (Fig. 1.4). One may have difficulty distinguishing them from widened cisterns or

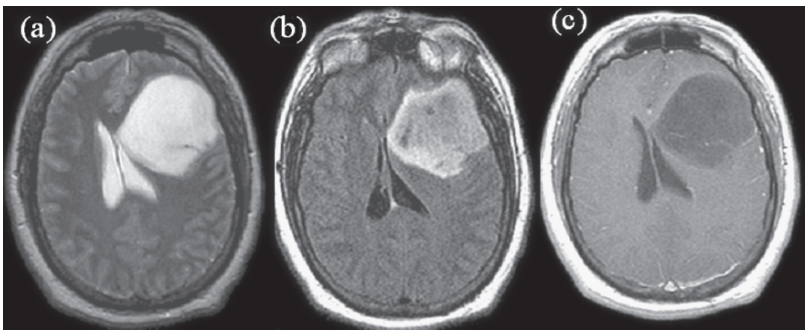

Fig. 1.4 Epidermoid cyst. Axial T2-weighted image (**a**) demonstrating a homogenously hyperintense mass in the left frontal lobe (**a**) that appears hyperintense on corresponding FLAIR image (**b**). The mass does not show any enhancement on the post contrast T1-weighted image (**c**)

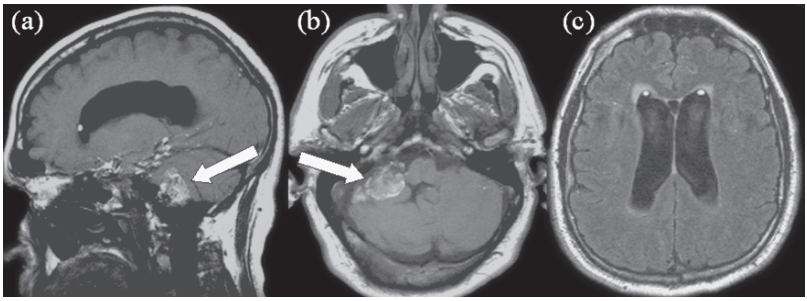

Fig. 1.5 Ruptured Dermoid cyst. Sagittal T1-weighted image (**a**) and corresponding axial T1-weighted image (**b**) demonstrating a hyperintense mass in the right cerebellopontine angle (arrows). Floating fat deposits within the lateral ventricles are visible on FLAIR image (**c**)

arachnoid cysts on standard spin echo sequences. The contrast between lesion and CSF may be improved by using a constructive interference in the steady state [33].

Dermoid cysts are generally midline lesions that contain oily material, which has a conspicuously bright signal on T1-weighted images. Since they are prone to rupturing into the CSF spaces, fat deposits floating on top of CSF may be seen in ventricles, cisterns, or sulci (Fig. 1.5). The keratinized components have a low signal on all imaging sequences. Colloid cysts are roundish masses that arise near the foramen of Monro and project into the third ventricle. If large enough, they cause obstructive hydrocephalus, which in pedunculated lesions can develop acutely. The MR appearance varies, depending on cyst content (hemosiderin, calcium, metal ions, lipids, cholesterol) [34].

2.1.2 Perfusion-Weighted Imaging

In brain tumors, perfusion-weighted imaging (PWI) measures the degree of tumor angiogenesis and capillary permeability, both of which are important biological markers of malignancy, grading and prognosis. Brain tumor vasculature plays a critical role in supplying nutrients and oxygen to tumor cells, and also provides a road map for tumor infiltration [35, 36]. Most widely used PWI methods include dynamic susceptibility contrast (DSC), dynamic contrast-enhanced (DCE) and arterial spin labeling (ASL).

Basic Principle of Perfusion Techniques

The most robust and widely used quantitative variable derived from DSC imaging is the relative cerebral blood volume (rCBV). It has been shown that, in the absence of re-circulation and contrast material leakage, rCBV is proportional to the area under the contrast agent concentration time curve. In general, the assumptions of

negligible re-circulation and contrast material leakage are violated in the presence of a tumor. The effects of this assumption can be reduced by fitting a gamma variate function to the measured signal intensity time curve [37]. Both spin echo (SE) and gradient echo (GRE) sequences can be used for measuring rCBV. SE techniques have been shown to be sensitive to small vessels, whereas GRE images incorporate signals from large vessels, including normal veins as well as tumor microvascularity [38]. A strong correlation between tumor grade and blood volume has been observed with GRE technique [39].

DCE-PWI consists of rapid and repeated T1-weighted images after a bolus injection of contrast agent (e.g., Gd-DTPA). The signal intensity on these sequential images is converted into contrast concentration using calculated or assumed T1 relaxation times. Using mathematical modeling and the signal intensity from the artery (arterial input function) the size of the extravascular extracellular space (EES) and endothelial transfer coefficient, K^{trans}, can be measured. The most widely used method is based on the pharmacokinetic model of Tofts and Kermode [40]. The estimated parameters are the permeability surface area product of the endothelium (PS), the fractional size of EES and the time course of blood plasma Gd-DTPA concentration or the arterial input function. While K^{trans} is widely used in DCE studies, it is affected by several hemodynamic factors such as blood flow, blood volume, endothelial permeability and endothelial permeability surface area.

In contrast to DCE imaging, endogenously labeled arterial water is used as a contrast agent in arterial spin labeling (ASL) techniques to measure tissue perfusion. The labeling of water protons is performed by application of a powerful magnetic field gradient to inflowing blood to invert its magnetization. The labeling can be implemented either with pseudo-continuous saturation or by flow-driven adiabatic inversion pulses [41, 42]. In an ASL experiment a pair of images are acquired, one in which blood and tissue water magnetization are different (spin labeled image), and another in which the two magnetic states are similar (control image). The perfusion parameters are then estimated from the subtracted image. Since water is used as an endogenous contrast (which being a small molecule is freely diffusible), the ASL methods are not confounded with the permeability issues faced when using the DSC or DCE methods [43] and, as such, provide a quantitative measure of perfusion. However, these methods suffer from poor signal to noise and relatively higher specific absorption rate.

Grading of Brain Tumors

Astrocytomas and rCBV

Gliomas are the most common type among primary tumors of the brain, with astrocytomas being the most common subtype. In astrocytomas vascular morphology is a critical parameter in determining malignant potential and survival. Several studies have shown a strong correlation between rCBV and astrocytoma grading [17, 44]. It is generally observed that as the grade of fibrillary astrocytoma increases, the

maximal rCBV tends to increase. However, it is still not clear as to what is the histological correlation of this increased rCBV. High-grade astrocytomas are characterized by a high level of histological variability, resulting in heterogeneous rCBV maps. On the other hand, low-grade astrocytomas tend to exhibit homogenous rCBV maps [45].

Non-astrocytic Gliomas and rCBV

Some low-grade non-astrocytic gliomas occasionally present with high rCBV. Oligodendrogliomas are well-known for their delicate neo-angiogenic vessels, which have been classically described as having a dense network of branching capillaries resembling a "chicken wire" pattern [46]. As such, low-grade oligodendrogliomas may demonstrate elevated rCBV that can be as high as that of GBM [47]. Choroid plexus tumors are gliomas that arise from the choroid plexus within the ventricular system of the brain. These are highly vascular tumors composed of capillaries derived from the choroid plexus, which does not contain a BBB. This results in very leaky capillaries, which causes avid enhancement on post-contrast T1-weighted images. On DSC- PWI, choroid plexus tumors demonstrate marked leakage of Gd-DTPA at the start of the bolus, and the signal intensity curve does not return to baseline levels during image acquisition. Thus, rCBV measurements of choroid plexus tumors tend to be markedly under or over-estimated [48]. A recent DCE study has also shown a strong correlation of rCBV with glioma grade [49].

Brain Tumors Other Than Gliomas and rCBV

Most meningiomas are biologically benign, WHO grade I tumors. The less common atypical meningiomas (WHO grade II) tend to be more clinically aggressive and are likely to recur even after complete resection. Regardless of grade, meningiomas are highly vascular tumors that usually derive their blood supply from dural vessels of the external carotid artery, though pial supply is not uncommon. Results from a recent preliminary study suggest that the type of vascular supply, dural or pial may affect the characteristics of the susceptibility-weighted signal intensity time curve. It was shown that a profound contrast leakage occurred during the bolus phase for meningiomas that derive their blood supply from dural vessels, compared with those tumors supplied by pial vessels. Although the validity of this observation has not been established, the concept of detecting the type of vascular supply to meningiomas by using DSC PWI has profound implications in selection of patients for preoperative embolization, which is limited to dural vessels compared to surgical planning for pial-supplied meninigiomas, which tend to bleed more during surgery [47].

Primary cerebral lymphoma (PCL) is a highly malignant brain tumor, usually of B-cell lymphocyte origin. PCLs can mimic malignant primary gliomas, metastatic brain tumors or even infection on anatomic MRI [50]. On DSC PWI, lymphomas tend to show elevated rCBV, but not to the same degree as GBM. This is probably due to the fact that florid angiogenesis is not a typical feature of PCL. Rather, PCL is well-known for its angiocentric histologic feature, in which the lymphoma cells

tend to center around preexistent brain vessels [51]. DSC PWI alone, however, may not provide accurate diagnostic differentiation between PCL and other types of malignant brain tumors. Metastatic brain tumors usually do not pose a diagnostic dilemma on MRI because they tend to be multiple, are located near the gray matter-white matter junction or the subarachnoid space, and often a known history of systemic malignancy is present. However, approximately 30 percent or more of all metastatic brain tumors can manifest as a single mass in the brain [52]. Common to all metastatic brain tumors is that their tumor capillaries do not resemble those of the brain, but of the organ where the systemic cancer arose [53]. Metastatic brain tumors contain capillaries that are highly leaky because the capillaries outside the brain do not possess the unique barrier function of the brain capillaries. This is reflected in the susceptibility-weighted signal intensity time curve where profound leakage of Gd-DTPA is noted in the early bolus phase. DSC PWI reportedly can be useful in differentiating primary high-grade gliomas from solitary metastatic brain tumors, where rCBV values within the vasogenic edema of metastases were significantly lower than those within the infiltrative edema of gliomas [54].

Glioma and K^{trans}

Endothelial permeability of vessels in brain tumors provides valuable information about BBB integrity, vascular morphology and the nature of neo-vascularization, as well as tumor pathophysiology and prognosis [55, 56]. Several recent studies have shown that quantitative estimates of microvascular permeability correlate with brain tumor grade [56-58].

K^{trans} from DCE imaging have been assessed in many clinical settings and have been shown to be useful in determining the glioma grade [58] and treatment response [59]. K^{trans} is a quantitative measure of the degree of increase in T1 due to accumulation of Gd-DTPA in tissue. Because higher-grade gliomas tend to demonstrate T1 enhancement after administration of Gd-DTPA, K^{trans} correlates strongly with glioma grade and histologic proliferative marker, MIB-1 index [49, 60, 61]. With increasing glioma grade, there is a higher likelihood of T1-weighted contrast enhancement of the tumor and, hence, increasing K^{trans}. Although K^{trans} derived from DCE MRI is commonly used at several institutions, an alternative method of perfusion imaging using the dynamic susceptibility contrast has also been proposed [62].

In brain tumors the blood flow to the tumor tissue is often hampered by an abnormal vasculature comprised of immature or defective endothelium, tortuosity and thrombosis. Hence, the uptake of Gd-DTPA by the tumor is mainly limited by blood flow and not by permeability. However, in inflammatory lesions such as a multiple sclerosis plaque, the limiting factor for uptake of Gd-DTPA is permeability and not blood flow. In addition to the complexity of pharmacokinetic modeling, the inherent heterogeneity of a brain tumor and its vasculature poses a significant challenge in permeability measurements and accurate interpretation of the data.

Glioma and Absolute CBF

Absolute or quantitative CBF values using ASL techniques have been used to characterize tumor grade [63, 64]. Wolf, et al. [63] reported accurate differentiation of high from low-grade gliomas in a study of 26 patients when excluding oligodendrogliomas. A recent study by Warmuth, et al. [64] compared the DSC method with ASL in primary and secondary CNS neoplasms, and reported that both are suitable for tumor grading. CBF measured from ASL provided similar information as rCBV measures generated with DSC-based perfusion MR methods (Fig. 1.6).

Differentiation of Gliomas from Metastases

Intracranial metastases and primary high-grade gliomas are two common brain tumors encountered in adults. The management of these two tumors is different and can potentially affect clinical outcome. Several reports have demonstrated significantly higher rCBV in peritumoral region of high-grade gliomas than that of metastases [54, 65]. This is possibly due to the fact that, in primary high-grade gliomas, peritumoral areas contain altered capillary morphology. These tumors also exhibit scattered tumor cells infiltrating along newly formed or preexisting, but dilated, vascular channels. In metastases, on the other hand, the peritumoral region contains no infiltrating tumor cells [66].

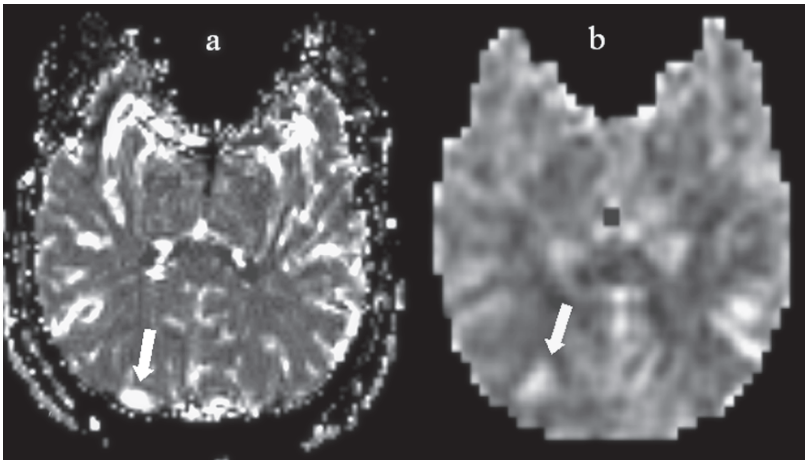

Fig. 1.6 Parametric maps from a high-grade glioma. Relative cerebral blood volume map (**a**) and cerebral blood flow map (**b**) demonstrate foci of high blood volume and blood flow respectively (arrows) within the mass in the right parieto-occipital lobe consistent with high-grade glioma

2.1.3 Diffusion-weighted Imaging

Diffusion-weighted imaging (DWI) is an imaging technique in which random microscopic water motion is responsible for the contrast generated within the image. The diffusion of water molecules in the brain is characterized by its apparent diffusion coefficient (ADC) and the extent of directionality by fractional anisotropy (FA). DWI has been established as a reliable non-invasive method for the early detection of cerebral ischaemic stroke [67]. In brain tumors, ADC values have been used to distinguish normal brain tissue from necrosis, cysts, edema and solid tumor. These differences are thought to result from changes in the balance between intracellular and extracellular water, and due to changes in the structure of the two compartments [68].

Basic Principles of Diffusion Technique

The DWI image is based on the principle that water molecules in any living tissue routinely undergo random motion. These images are typically obtained by measuring the loss of signal after a pulse that consists of a pair of diffusion gradients added on either side of the 180° pulse of a SE sequence. This sequence can be combined with different readout strategies, like echo planar imaging or spiral imaging. The degree of MR signal attenuation after application of the diffusion gradients depends upon the duration and strength of the magnetic field gradients and the diffusion coefficient of the tissue (D). The degree of signal loss can be represented by the term S/S_0, in which signal after the application of diffusion gradients is represented by S, and signal before by S_0. The ratio of S/S_0 is proportional to the exponential of the diffusion coefficient (D) and the degree of diffusion weighting (b), and is represented as: $S/S_0 \propto \exp(-b*D)$ [69].

Grading of Gliomas

Among the histological features used for glioma grading, cellularity has been the target of quantitative assessment with DWI. Translational movement of water molecules occurs in the extracellular space and any increase in swelling or cellularity causes a drop in ADC values. Hence, the higher the glioma's grade, the lower the mean tumor ADC values [70-74] (Fig. 1.7a). Various attempts have been made to use ADC values for predicting the glioma grade, however, the results have been conflicting [75-78]. In a recent study, Fan, et al. [78] reported a significantly lower ADC value in solid portions of high-grade gliomas ($0.52 \pm 0.11 \times 10^{-3}$ mm^2/s), compared to low-grade gliomas ($1.15 \pm 0.16 \times 10^{-3}$ mm^2/s). However, Yang, et al. [75] reported that ADC values in low-grade tumors were lower than high-grade. Other studies have failed to observe any difference between the two grades of tumors [76, 77]. The limited role of ADC in glioma grading is likely due to the inherent heterogeneity associated with gliomas across different grades, within the same grade, and even within a single tumor.

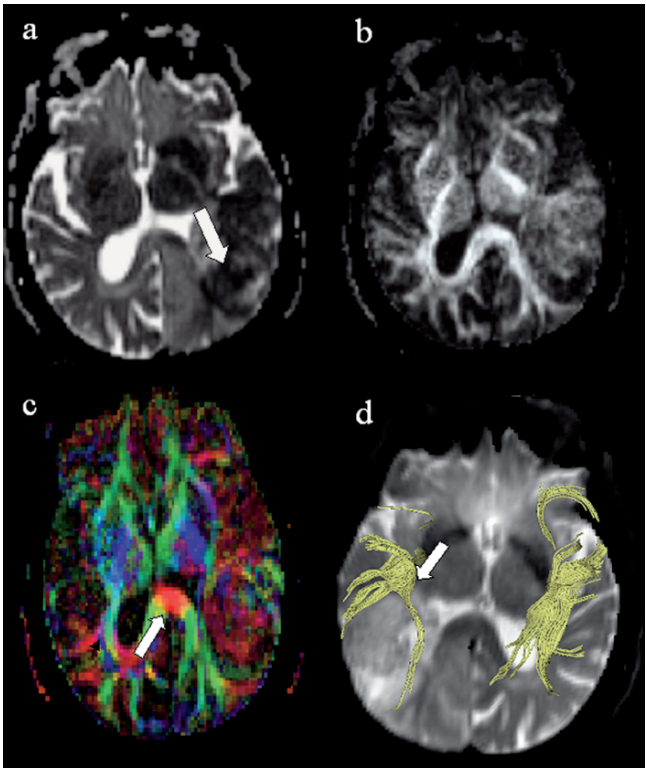

Fig. 1.7 Diffusion parametric maps from a high-grade glioma. Axial ADC map (**a**) demonstrates restricted diffusion within the mass in the left parietal region extending into the lateral ventricular system (arrow). Corresponding FA map (**b**) demonstrates reduced anisotropy. Directionally encoded color map (**c**) showing displacement and infiltration of superior longitudinal fasciculus (arrow). Color indicates directions as follows: red, left-right; green, anterior-posterior; blue, superior-inferior. Fiber tracking image (**d**) shows diminished superior longitudinal fascicular fiber in the cerebral hemisphere involving the tumor compared to the contralateral side (arrow) (top view)

Another application of DWI in brain tumors is the use of fractional anisotropy (FA) maps derived from diffusion tensor imaging (DTI) in determining the integrity of white matter tracts in the vicinity of the tumor (Fig. 1.7b). Although there is a lack of direct histological correlation between FA maps and the status of white matter tracts near the tumor, a variation of FA matrices, such as the tumor infiltration index [79] or fiber attenuation index [80], may provide more specific information on the status of peritumoral edema in brain tumors. FA has been suggested as a good predictor of cell density and proliferation of GBMs [81]. However, the biological correlates for the DTI-derived matrices remain unclear and await much needed histological validation.

Differentiation of Gliomas from Metastases

Krabbe, et al. [82] reported ADC values for metastases ($1.2\text{-}2.73 \times 10^{-3}$ mm^2/s) and high-grade gliomas ($0.72\text{-}2.61 \times 10^{-3}$ mm^2/s) which were not significantly different. Similarly, Kono, et al. [74] did not report any differences in ADC values between the two types of tumors using a larger patient population. These studies show that ADC values from solid enhancing portions of metastases are not useful in the differentiation from markedly enhancing high-grade gliomas. However, several studies have demonstrated the utility of DWI in differentiating these two entities when ADC values were measured from peritumoral regions, with some studies reporting significantly higher peritumoral ADC in metastases than that of gliomas [77, 83].

Tumor Types and ADC

In a study of 48 patients with contrast-enhancing malignant tumors, significant differences in the ADC_{min} values were noted between lymphomas and GBM, and between lymphomas and anaplastic astrocytomas (AA). However, there were no differences between lymphomas and metastases, and between GBM, AAs and metastases [84]. On the other hand, Krabbe, et al. [82] did not observe any significant differences in the mean ADC values in patients with meningiomas, compared to high-grade gliomas or brain metastases.

ADC values have also been correlated with cellularity of non-glial brain tumors. When compared with gliomas, lymphomas and medulloblastomas were shown to have lower ADC values because of densely packed cells in these tumors [85]. In a small sample of meningiomas, malignant or atypical meningiomas were found to have lower ADC values when compared with typical meningiomas [86].

2.1.4 White Matter Tractography

Diffusion tensor imaging (DTI) is distinguished from DWI by its sensitivity to anisotropic or directionally dependent diffusion of water molecules. The anisotropic diffusion in the brain is largely attributed to the cytoarchitectural compositions of myelin and axons. DTI requires collection of diffusion data in at least six non-collinear directions. Anisotropic diffusion is characterized by a tensor, which fully describes the mobility of the water molecules in each direction and the correlation between them. The tensor can be diagonalized such that only the three non-zero elements, known as the eigen values, remain along the diagonal of the tensor. Each eigen value is associated with an eigenvector where the largest of the three eigen values corresponds to the principle eigenvector and describes the principal direction of diffusion at that point. As shown in Fig. 1.7c, by choosing the eigenvector associated with the largest eigen value, the principal diffusion direction of the brain structure to be examined can be color-coded, resulting in color-coded maps or directionally encoded FA maps [69].

In fiber tractography with DTI, white matter tract directions are mapped on the assumption that in each voxel a measure of the local fiber orientation is obtained.

Fiber tracking provides a 3-D depiction of white matter connectivity, which allows studying brain cytoarchitecture at a microscopic level. DTI-based fiber tractography necessitates definition of a seed region of interest (ROI) that is located at the path of the investigated fiber network system to initiate the fiber tracking process [87]. Selecting seed ROIs based on known anatomical landmarks has led to the identification of a large number of fiber bundles in healthy subjects [88, 89].

In patients with brain tumors, tractography enables visualization of specific fiber bundles that are either in proximity to a tumor or that are influenced by it. This information helps in intra-operative guidance for tumor resection [90]. Tractography maps of desired white matter tracts can be overlaid onto high-resolution anatomic images, and provide information on alterations in fiber tract directionality and integrity due to the presence of a brain tumor (Fig. 1.7d).

Tractography of the corticospinal tract (CST) is beneficial for pre-surgical planning as it helps the surgeon to avoid injuring the CST during tumor resection. The role of DTI in brain tumors was recently evaluated in nine patients with eight gliomas and one metastatic adenocarcinoma [91]. The white matter tracts were characterized as being displaced, edematous, infiltrated or disrupted. Nine large white matter pathways in five patients were displaced; two patients with frontal oligodendrogliomas showed infiltration (confirmed pathologically). The investigators concluded that DTI is beneficial in pre-surgical planning, but it was not clear as to whether resection of anatomically intact fibers in abnormal-appearing areas of the brain would lead to postoperative deficits. In a separate study, DTI was used to determine abnormalities beyond those seen in T2-weighted scans on patients with low- and high-grade gliomas and metastases [92]. Abnormalities on DTI were larger than those seen on T2-weighted images in 10 out of 13 patients with high-grade gliomas, but not in metastases or low-grade gliomas. Furthermore, four out of 13 of these cases showed new abnormalities in the contralateral hemisphere, suggesting the possibility of tumor spread across the corpus callosum. The implication of this study is that DTI can improve the targeting of radiation therapy to visible tumor volume, as well as encompassing ‘invisible’ tumor infiltrating the white matter pathways. Another potential application of this technique is in distinguishing between normal white matter, edematous brain and enhancing tumors, as reported in a study of nine patients with GBMs [93]. This technique may also be useful in tracking the distortion of white matter pathways by low-grade gliomas, and anticipating the development of neurological impairment due to the presence of tumors.

2.1.5 Proton Magnetic Resonance Spectroscopy

Basic Principle of MRS

Similar to the basic principles of MRI, MRS is based on the spin properties of atomic nuclei (e.g. ^{1}H, ^{31}P, ^{13}C, ^{19}F) when present in a strong magnetic field, that allows the nuclei to absorb and re-emit energy in response to a radio frequency pulse at the resonance frequency of that particular nuclei. The effective magnetic field, sensed by a particular nucleus, is affected by neighboring electrons. The separation of resonance

frequencies of different protons of a molecule due to the dissimilar chemical environment is described as the chemical shift (δ), and is expressed in parts per million (ppm). The height (maximum peak intensity) or the area under the peak yields relative measurements of the concentration of protons.

The spectral information from a particular region of the brain is generally obtained by spatial localization, which is achieved by applying static and/or pulsed gradients. Localization methods commonly used in clinical ^{1}H MRS include: point-resolved spectroscopy (PRESS), spatially resolved spectroscopy (SPARS) and the stimulated echo method (STEAM). As abundant water protons (70 M) impose limitations to observe intracellular metabolites (1-10 mM), the signal from water needs to be suppressed. The most frequently used method for suppressing the signal from water is chemical shift selective excitation (CHESS), which reduces the water signal by a factor of 1,000 [94].

Biochemical Features of a Normal Human Brain Spectra

The most prominent resonances that are seen from normal human brain on in vivo ^{1}H MRS include N-acetyl aspartate (NAA), together with intense signals from creatine (tCr), choline-containing compounds (tCho), myo-inositol and multiple peaks from glutamate and glutamine (Glx) (Fig. 1.8).

Biochemical Features of Tumor Spectra

NAA (singlet at 2.02 ppm) is mainly distributed in intact neurons and neuronal processes such as axons. Studies on cultures of separated brain cells have revealed the presence of NAA in un-differentiated oligodendrocyte cells as well [95]. However, presence of NAA in mature oligodendrocytes and astrocytes is generally

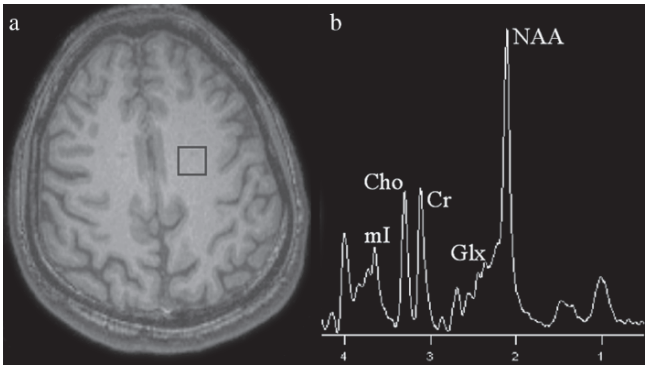

Fig. 1.8 Proton magnetic resonance spectrum from a normal brain. Axial T1-weighted image (**a**) demonstrating voxel position at the centrum semiovale. ^{1}H MRS spectrum (**b**) acquired with PRESS sequence displaying characteristic resonances [NAA (2.02 ppm); tCr (3.03 ppm); tCho (3.22 ppm); Glx (2.35 ppm) and mI (3.56 ppm)] from the voxel shown in (**a**)

not observed. The acetyl group of NAA has been suggested to have a role in biosynthesis of lipids, while the aspartyl group is involved in metabolism of several neurotransmitters [96]. NAA has generally been found to be either absent or reduced in brain tumors [97].

Total choline (tCho, single peak at 3.22 ppm comprising signals from choline, phosphocholine and glycerophosphocholine) is elevated in tumors, compared to normal brain tissue [97, 98]. Increased tCho is thought to be present due to accelerated membrane synthesis of rapidly dividing cancer cells. In vivo tCho levels have been shown to correlate with proliferative potential of the tumor as determined by immunohistochemical analysis of tumor biopsies using the Ki-67 labeling in gliomas [99] and meningiomas [100]. However, meningiomas, which are mostly benign and slow growing, can have tCho concentrations comparable to grade III astrocytomas [101].

Creatine-containing compounds (tCr; peak at 3.03 comprising signals from creatine and phosphocreatine) is reduced in astrocytomas, compared to normal brain tissue and is almost absent in meningiomas [98], schwannomas [102] and metastases [103]. Creatine-containing compounds are thought to have a role in maintaining energy-dependent systems in brain cells by serving as a reserve for high-energy phosphates. Creatine-containing compounds also serve as a buffer in adenosine triphosphate and adenosine diphosphate reservoirs as it is increased in hypometabolic states and decreased in hyper-metabolic states [104].

Myo-Inositol (mI; singlet at 3.56 ppm) has a short T2 and as such can only be observed with sequences using a short echo time (TE). Myo-Inositol is mostly found in astrocytes [97] and is high in low-grade gliomas [98, 105], but low or absent in non-glial tumors such as schwannomas [102] and meningiomas [98]. Higher levels of mI have been reported to distinguish hemangiopericytomas from meningiomas [106]. This metabolite is also a precursor for lipid metabolism and, hence, may be elevated due to increased cellular proliferation. Some studies suggest its role as an osmolyte and have attributed its increase in inflammatory processes [107].

The broad multiplet signals (between 2 and 2.4 ppm, and 3.76 ppm) from glutamate and glutamine (Glx) are most readily observed at short TE. Glx is prominently observed in meningiomas, possibly reflecting altered energy metabolism involving partial oxidation of glutamine leading to alanine (Ala, doublet at 1.47 ppm), which is also elevated in meningiomas [98, 101]. Glutathione (GSH; multiplets at 2.9 and 3.8 ppm) is part of the same metabolic pathway, and has been recently identified by in vivo ^{1}H MRS and is reported to be higher in meningiomas, compared to astrocytomas [108].

Lactate (doublet at 1.33 ppm) is frequently observed in tumors, probably due to increased anaerobic glycolysis [109], and is often most prominent in high-grade tumors. However, studies have reported that lactate levels do not correlate with tumor grade [110] or metabolic rate [111]. Lactate is present in both intracellular and extracellular spaces, and its overall concentration is dependant upon metabolic rate of cells and clearance from the cell and the interstitium. A reduced clearance rate in necrotic or cystic regions leads to increased lactate levels, independent of any increase in glycolysis associated with high-grade tumors [110].

Lipids (0.9 and 1.3 ppm) are also characteristic of high-grade tumors at short TE [98, 112], but are only observed in about 41 percent of high-grade tumors [7]. Biopsy studies indicate that lipids correlate with necrosis [113], which is a histological characteristic of high-grade tumors. Increased lipid signals in tumors could be the result of membrane phospholipids released during cell breakdown, and may thus relate to the necrotic fraction. Studies in animal models suggest that triglycerides are stored as droplets in the cytosol as a result of hypoxic stress [114], and the presence of lipid resonances at 2.8 and 5.4 ppm have also been proposed as markers of apoptosis [115].

Grading of Gliomas

As shown in Fig. 1.9, both single voxel ^{1}H MRS and multivoxel proton magnetic resonance spectroscopic imaging (^{1}H MRSI) have been used to evaluate the degree of malignancy of brain tumors [75, 116-118] (Fig. 1.9). The most common observation in grading of glioma is that the tCho/tCr and tCho/NAA ratios increase with grade; however, there is a significant overlap of these indices between grades, most likely due to the heterogeneity of tumors. Kaminogo M, et al. [119] reported that tCho/NAA was less than 1.0 in healthy tissues and greater than 1.0 in all but one of the gliomas studied. The tCho/tCr ratio tended to be higher with higher histological grades. A significant difference was observed between grades II and IV, but not between grades II and III or III and IV. Recently short TE data have shown a decrease in mI/tCr and mI/tCho with grade [98, 105]. Meyerland, et al. [9] reported that Lac/Water is useful in grading of gliomas. Some studies have also indicated that lipids play a role in grading of high-grade tumors [98, 112].

Since most tumors are heterogeneous, their spectra are likely to have contributions from multiple tissue compartments [120]. Along with viable tumor cells, there

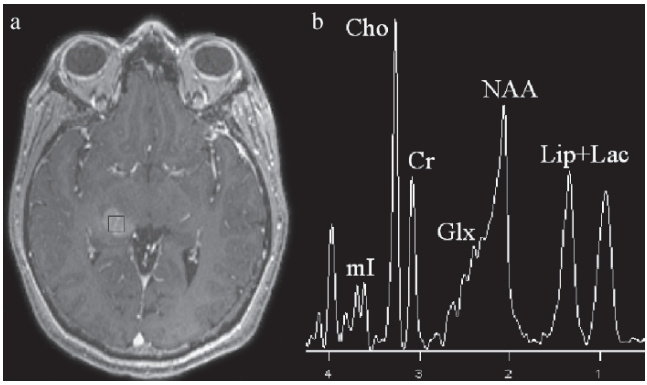

Fig. 1.9 Proton magnetic resonance spectrum from a high-grade glioma. Axial post-contrast T1-weighted image (**a**) showing homogenously enhancing mass in the right medial temporal lobe demonstrating the position of a voxel. Proton magnetic resonance spectrum (**b**) from the voxel shown in (**a**) exhibiting typical spectral features of a high-grade glioma. Note the reduced NAA and abnormally elevated peaks of tCho and Lip+Lac

may be necrotic and cystic regions, and in the case of highly infiltrative tumors there may also be contributions from normal brain tissue. Additionally, tumor growth is not well regulated and as such variations in cellular metabolism and cell density will occur, and as a tumor progresses it may become composed of cells of different grades [121]. Because of heterogeneous characteristics of tumors, accurate grading of gliomas has not been completely achieved by ^{1}H MRS [7, 106, 122-124].

Differentiation of Gliomas from Metastases

^{1}H MRS has shown a great potential in differentiating high-grade gliomas from metastases, particularly when the lesion is solitary and conventional MRI is inconclusive. Ishimaru, et al. [103] reported elevated tCho from enhancing portions of all the high-grade gliomas and metastases studied. They also reported an absence of tCr and NAA in most of the metastases, indicating that the absence of these resonances could be used for differentiating them from gliomas. The absence of tCr in metastases may be the result of exhaustion of energy reserves due to a rapid cell proliferation, compared to gliomas. A study with a larger population – 51 patients – with a solitary brain tumor (33 gliomas, 18 metastases) has reported significantly elevated tCho/tCr in the peritumoral region of gliomas (2.28 ± 1.24), compared to metastases (0.76 ± 0.23) [54]. However, there was no significant difference in peritumoral NAA/tCr between the two groups, as there is no neuronal replacement or destruction in the peritumoral regions in either pathologic condition. It has been shown that in high-grade gliomas, tumor cells infiltrate along vascular channels but do not destroy the preexisting cytoarchitecture [17]. Vasogenic edema associated with metastases is also a passive process that does not necessarily destroy the underlying structure or neuronal tissue [125].

2.1.6 Multiparametric Analysis

Histologically, gliomas often demonstrate considerable heterogeneity, with focal areas of malignant features dispersed over several regions. Due to this inherent heterogeneity, MRI techniques such as PWI, DWI and ^{1}H MRS, when used independently, often lead to ambiguous results in grading of gliomas, specifically oligodendrogliomas [7, 106, 122-124]. The preexisting heterogeneity may also be the reason for overlapping rCBV and metabolite ratios between different glioma grades [126]. Limited studies have been performed to combine advanced MR techniques to more accurately characterize and predict survival of brain tumors. This approach offers detailed and complementary information on the complicated intra- and peritumoral architecture that reflects tumor vascularity, cellularity and metabolic information. Combined measurement of rCBV, ADC and ^{1}H MRS indices has been shown to improve the sensitivity and specificity of glioma grading [116], and for the characterization of brain metastases [65] Figs. 1.10 through 1.12 demonstrate multiparametric analysis from representative cases of high-grade glioma, low-grade glioma and metastasis, respectively. Multiple MRI and ^{1}H MRS techniques may

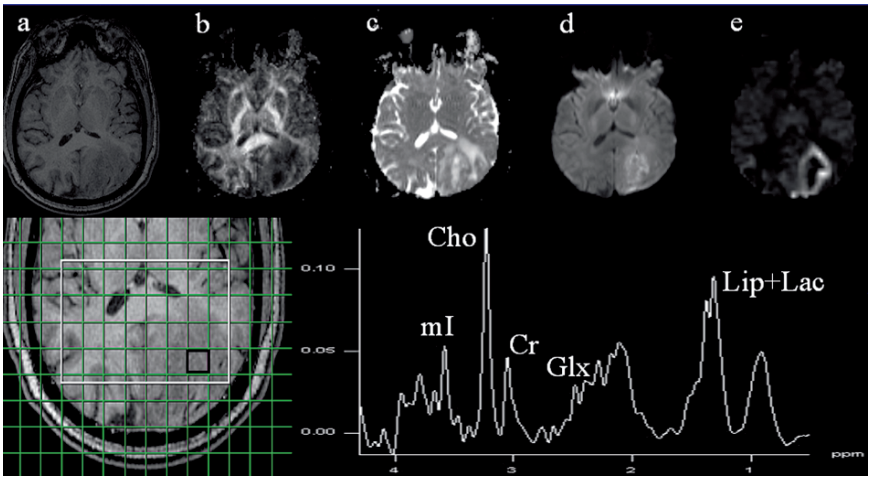

Fig. 1.10 Multiparametric analysis from representative case of a high-grade glioma. T1-weighted image (**a**) demonstrating a diffusely hypointense mass with surrounding edema in the left parieto-occipital region. Co-registered FA map (**b**) showing regions of reduced anisotropy. Corresponding ADC map (**c**) and DWI image (**d**) demonstrating heterogeneous diffusion within the mass. Increased perfusion with a ring of high blood flow on CBF map (**e**) indicative of a high-grade glioma. Two-dimensional CSI grid overlaid on T1-weighted image (lower panel) showing a representative voxel (black) and corresponding spectrum exhibiting various metabolites. Resonances of high Lip+Lac and tCho are consistent with findings of high-grade glioma

provide a more accurate assessment of brain tumors, providing useful information for guiding stereotactic biopsies, surgical resection and radiation treatment. Composite information from all relevant techniques is desirable as it is unlikely that all parameters will be useful in every patient or at every time-point. Multiparametric analysis also provides quantitative and correlative measurements that are closely related to the biological properties of the tumor, and reflect changes in tumor vascularity, cellularity and proliferation that are associated with tumor progression. Gupta, et al. [71] have previously reported a significant inverse correlation between tCho and ADC in gliomas. This study suggested that tumor cell density plays a major role in defining the level of tCho signal. Some studies have shown that there is a strong correlation between high vascularity (high rCBV), increased cellularity (low ADC) and increased membrane turnover (high tCho) in gliomas [65, 75].

2.1.7 Functional Magnetic Resonance Imaging

One of the principal surgical goals for the treatment of brain tumors is to minimize neurological deficits and to maximize resection of the pathological mass. To achieve this goal, functional eloquent brain areas must be identified. The standard methods used for identifying these areas are intra-operative mapping in the conscious patient, implantations of a subdural grid with extraoperative stimulation mapping

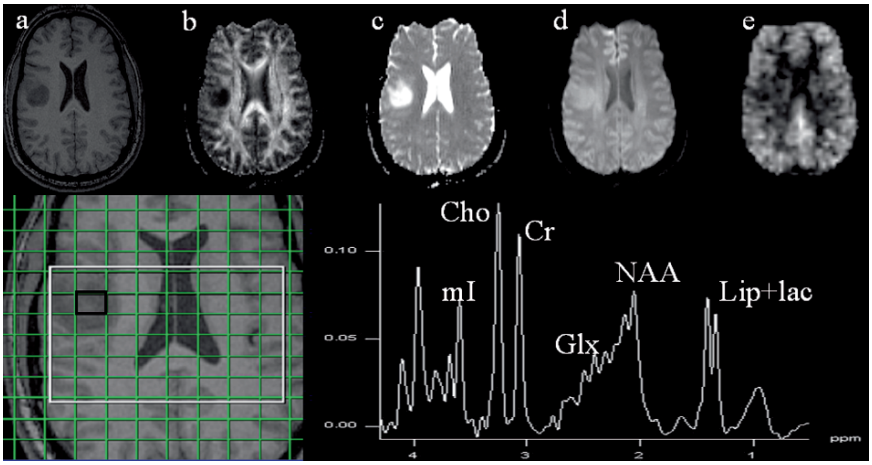

Fig. 1.11 Multiparametric analysis from representative case of a low-grade glioma. T1-weighted image (**a**) demonstrating a well-defined hypointense mass in the right parietal lobe with little peritumoral edema extending into the cortex. Co-registered FA map (**b**) showing low anisotropy. Corresponding ADC map (**c**) and DWI image (**d**) demonstrating high diffusivity indicative of low-grade glioma, which is also confirmed by low blood flow on the CBF map (**e**) (arrow). Two-dimensional CSI grid overlaid on T1-weighted image (Lower panel) showing a representative voxel (black) and corresponding spectrum exhibiting various metabolites. Note lower tCho/tCr ratio and lower level of Lip+Lac compared to high-grade glioma (Fig. 1.10)

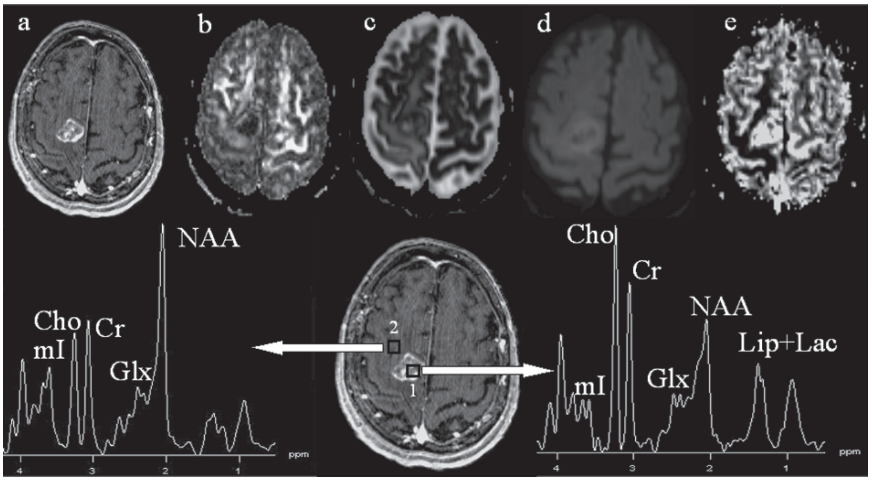

Fig. 1.12 Multiparametric analysis from a representative case of metastasis. Post-contrast T1-weighted image (**a**) demonstrating an enhancing mass in the posterior right frontal lobe. Co-registered FA map (**b**) showing low anisotropy, ADC map (**c**) and DWI image (**d**) showing high diffusivity from the core of the mass and lower diffusivity from the rim. Markedly elevated blood volume is visible only from the central core of the mass on rCBV map (**e**) whereas in the peritumoral regions, volume is low. Lower panel depicting 2D CSI grid overlaid on T1-weighted image showing representative voxels from tumoral (1) as well as peritumoral (2) region. Corresponding spectra exhibiting various metabolites. Note elevated Lip+Lac and tCho peaks only from the tumor region suggesting a case of metastasis

or operative sensory-evoked potential recordings. However, these techniques are invasive, induce extreme stress on the conscious patient, and often require a craniotomy larger than what is necessary for tumor resection.

fMRI is a non-invasive method that can be used pre-operatively and helps in establishing the relationship between the margins of the tumor and the functionally viable brain tissue. It is based upon the blood oxygenation level-dependent (BOLD) effect [127, 128]. It is believed that when the patient is asked to perform a certain language or motor task, the activation of neurons leads to an increase in oxygen consumption of these neuronal cells, which in turn induces a concomitant exaggerated increase of the local blood flow [129]. The decreased concentration of deoxygenated hemoglobin induces a higher signal on T2-weighted images, highlighting the functional areas of the brain relative to the task performed by the patient [130].

As the BOLD signal change following stimulation is relatively small, detection of a reliable change in activation is challenging. A number of post-processing steps like motion correction and smoothing of the data are required to accurately discern the functionally activated voxels. Functional maps are usually generated through a voxel-by- voxel statistical analysis of the time series MRI data. However, statistical procedures for preoperative mapping have not been standardized, as there is no consensus on the best statistical model for such studies or on the estimation of significance levels. Some authors apply a Bonferroni correction [16, 131], some put minimal thresholds on cluster sizes [132-134], while others perform permutation testing to estimate significance levels [135].

Influence of Tumors on BOLD Signal

Evidence indicates that the BOLD response in the vicinity of certain tumors does not reflect the electrical neuronal activity as accurately as it does in healthy brain tissue [136-138]. Recent data indicate that cortical BOLD activation can be reduced near glial tumors, both at the edge of the tumor and in normal vascular territories, somewhat removed from the tumor. Loss of regional cerebral vasoactivity near these tumors has been suggested to be a contributing factor [139]. At the interface of tumors and normal brain, astrocytes and macrophages can continuously release nitric oxide that leads to a regionally increased cerebral blood flow and decreased oxygen extraction fraction during basal metabolism. These processes may result in a decreased BOLD signal intensity difference following activation [139]. Holodny, et al. [137] found that the number of activated voxels was 35 percent less at the tumor site, compared to the contralateral site. The authors suggested that this is possibly due to loss of autoregulation and a changed venous response, due to compression of the neighboring vasculature by the presence of a tumor.

The presence of a tumor in the brain also leads to changes in regional tissue pH, glucose, lactate and adenosine triphosphate levels, although such effects on BOLD neuronal coupling have not been completely understood [140]. Glial tumors can induce abnormal vessel proliferation in adjacent normal brain tissue, altering regional CBF, rCBV, vasoactivity and, potentially, BOLD contrast. Other factors,

including vasogenic edema and hemorrhage, may also contribute to the observed decrease in the near-lesion BOLD contrast. Evidence for a substantial impact of vasogenic edema on BOLD contrast is lacking due to the small number of patients included in several of these studies. Micro-hemorrhages associated with intra-parenchymal tumors could hinder the detection of change in susceptibility gradients that provide BOLD contrast. Various pharmacological agents used in the treatment of tumors may also influence the BOLD signal. There are indications that antihistamines reduce and that caffeine boosts the BOLD response [141]. It has also been reported that levodopa modifies the BOLD response [142].

Presurgical fMRI in patients with brain tumors is a promising clinical application as it allows risk assessment of therapeutic interventions, selection of patients for intra-operative mapping and guides brain surgery. Unfortunately, no randomized trials or outcome studies have been performed to evaluate the role of pre-surgical fMRI in determining the final outcome of the patient. Therefore, fMRI has not yet reached the status of routine clinical acceptance. Combining pre-surgical fMRI with other techniques such as DTI may aid in greater use of fMRI in clinical brain tumor applications.

Combined Use of fMRI and Tractography

BOLD-fMRI and diffusion tensor tractography (DTT) may help in establishing the relationship between brain motor cortex, pyramidal tracts and gliomas, which might aid in optimizing surgical planning and guide microsurgery [143, 144]. Knowledge of the structural integrity and location of eloquent white matter tracts relevant to brain tumors is crucial in neurosurgical planning because damage to these clinically eloquent pathways can result in postoperative neurological deficits as devastating as damage to functional cortical areas.

In many brain tumor cases partial or no loss in functional activity is observed leading to the assumption that the fibers, though deviated, are still partially functionally intact. In such cases white matter mapping using seed ROI based on known normal anatomical landmarks might be misleading, since the white matter is deviated from its normal location. This task becomes even more complicated when edema, tissue compression and degeneration are present. These changes deform the architecture of the white matter and, in some cases, prevent accurate selection of the seed ROI from which fiber tracking begins. Recently, it has been shown that selection of the seed points based on fMRI activations, which constrain the subjective seed ROI selection, enabled a more comprehensive mapping of fiber systems [145].

3 Differentiation of Recurrent Tumor from Radiation Necrosis

Surgical resection of brain tumors is generally followed by chemo-radiotherapy that leads to radiation-induced necrosis. Despite aggressive and combined therapeutic regimes, brain tumors generally recur at or near the site of initial resection.

Differentiating radiation necrosis from recurrent tumor has important implications for the patient's management since recurrent tumors may benefit from repeat surgery with adjunct chemotherapy, whereas radiation necrosis may be treated with steroids. However, the distinction of delayed radiation-induced necrosis from tumor recurrence by using conventional MRI has been difficult [146]. Both entities manifest mass effect with surrounding edema. Both processes can cause varying degree of BBB disruption that results in abnormal contrast enhancement. Early radiation necrosis is characterized by fibroid necrosis of blood vessel walls, followed by necrosis of surrounding parenchyma. Late vascular changes include wall thickening, hyalinization and telangiectasia. Extensive reactive gliosis, dystrophic calcification and cyst formation are commonly observed adjacent to the necrotic foci [147]. On the other hand, a recurrent tumor is characterized by angiogenesis [17]. Several advanced MRI techniques such as ^{1}H MRS [148-151], PWI [17, 152] and DWI [153] have been used independently or in combination to differentiate tumor recurrence from radiation necrosis (Fig. 1.13).

The typical change that occurs on ^{1}H MRS of a tumor after radiation therapy is a reduction of tCho with a possible increase in lactate and/or lipids indicating the transformation of viable tumor cells towards necrosis [100]. Many groups have investigated whether the ^{1}H MRS pattern is sufficiently different to distinguish between the two groups [148-151]. Although these studies concluded that ^{1}H MRS is useful in accessing potential recurrence, there is a disagreement about a characteristic spectral pattern for either entity, since both decreases and increases in tCho have been reported post treatment. Some groups have reported that NAA and lactate can be used as reliable indicators of radiation change [150]. The difficulty lies in the fact that irradiated tumor beds usually contain a mixture of both tumor and radiation effects. In many studies, the voxel size used was too large, which led to partial volume effect from normal tissue.

Using PWI, it has been reported that rCBV, a surrogate marker of angiogenesis, allows differentiation between the two lesions. Tumor recurrence is generally associated with elevation of rCBV, compared to patients with radiation necrosis [17, 152]. Moreover, DWI detects therapy-induced water diffusion changes and has been useful in differentiating between these two conditions [153]. Asao, et al. [154] have found significantly lower ADC values in recurring tumors than in tumors with radiation necrosis.

3.1 MRI in Stereotactic Biopsy

Stereotactic biopsy (SB) has evolved as a powerful and safe tool to provide tissue diagnoses with minimal disruption of normal brain function. Sampling error in biopsies of high-grade gliomas is well-known and is partly attributable to heterogeneity within a single tumor [155, 156]. The rate of conclusive histopathologic diagnosis by SB is highly variable, ranging from 60 percent to 98 percent. Furthermore, it has been recognized that the tiny amounts of tissue obtained by stereotactic biopsy may not be sufficient for a correct diagnosis, and may lead to errors that can have an impact on therapeutic management [157].

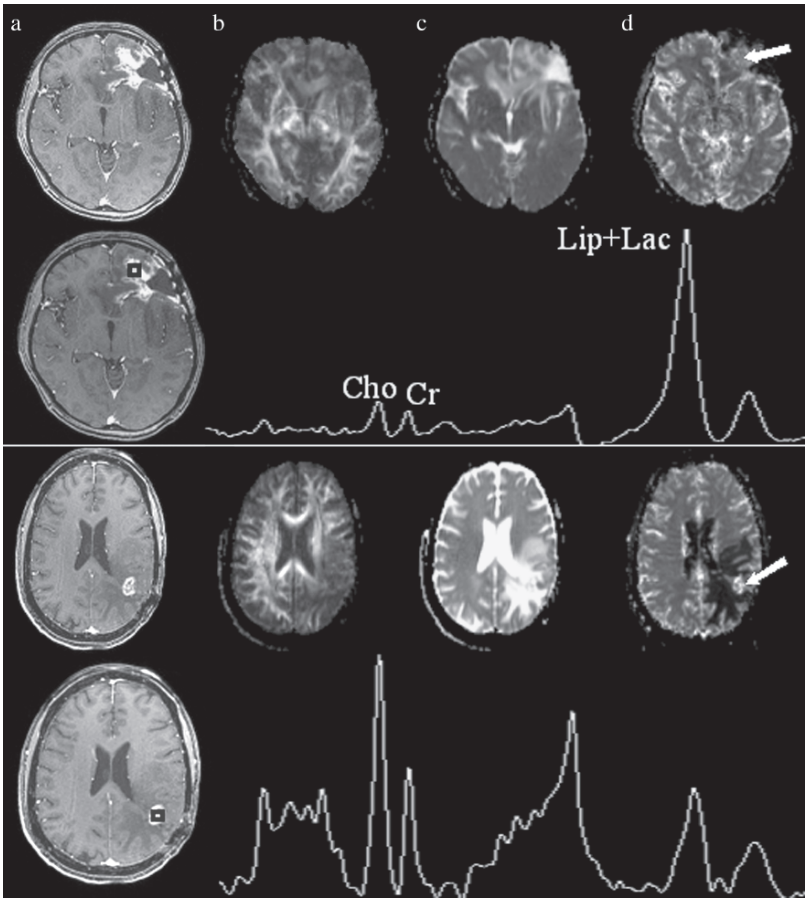

Fig. 1.13 Multiparametric analysis to differentiate tumor recurrence from radiation necrosis. Post-contrast T1-weighted images (**a**) showing contrast-enhanced masses in patients with radiation necrosis (upper panel) and tumor recurrence (lower panel). Co-registered FA (**b**), ADC maps (**c**) showing reduced anisotropy and elevated diffusivity within the mass in both patients. However, co-registered rCBV maps (**d**) demonstrating lower perfusion in patient with radiation necrosis compared to tumor recurrent patient (arrows). Proton spectra from the voxels shown on contrast enhanced T1-weighted images (**a**) showing higher tCho and lower Lip+Lac in patient with tumor recurrence compared to radiation necrosis

A few reports have shown that MRI-guided stereotactic biopsy specimen accurately represents the grade of glioma. The grading of gliomas is based on histologic evaluation of specimens from the most malignant region of the tumor. Most biopsies are guided by contrast-enhanced T1- weighted images [158], which depict areas of BBB breakdown and may not indicate the most malignant or vascular portion of the tumor. On the other hand, rCBV maps depict foci of greatest vascularity, which corresponds to the regions of maximum malignancy and can aid in directing precise stereotactic biopsy, particularly in non-enhancing tumors [159].

^{1}H MRSI has also been reported to be useful for stereotactic procedures and has demonstrated a potential to overcome the limitations of a single voxel study by encompassing the tumor as well as the normal brain. Pathological specimen taken from areas of increased tCho/tCr ratios and decreased NAA/tCr ratios can facilitate diagnosis by demonstrating increased cellularity and mitoses [160].

3.2 MRI in Experimental Brain Tumor Models

To understand brain tumor biology and to develop new treatment strategies, several experimental animal models (especially rodents) of glial tumors have been developed over the past several years [161, 162]. These experimental brain tumor models are aimed towards development of new radiotracers for cellular proliferation and protein synthesis, characterization of tracers and detection of early responses to therapeutic interventions [115]. Strategies for imaging transcriptional regulation and migration of tumor cells, and imaging expression of exogenous genes that carry a marker or therapeutic function, for the purpose of developing improved gene therapeutic vectors, have become possible with the help of MRI of animal models [163, 164].

In recent years stem cell therapy has proven to be a promising means to improve neurological function in brain tumor pathologies and has excellent potential to be clinically effective on a large scale [165]. With cell-specific MRI, the distribution and survival of magnetically labeled stem cells has been monitored [166].

In vivo detection of tumor cell migration, establishment of in vivo assays for tumor-specific signal transduction pathways, assessment of tumor-specific antigens and of labeled bone marrow-derived endothelial precursor cells has been greatly facilitated by combining MRI methods with animal models [167-171].

The combination of MRI techniques and specific animal tumor models has provided opportunities to characterize the tumor microenvironment, and physiology, and to understand their impact on tumor growth [172, 173]. Using rodent models, it has been shown that novel imaging techniques like T1 rho-weighted imaging has better demarcation potential for tumor borders than proton-density or T2-weighted imaging, which could be useful in treatment planning when combined with other imaging sequences [174].

Imaging of animal models has great implications especially when molecular, diagnostic and treatment modalities have to be translated from the bench to bedside.

4 Positron Emission Tomography

PET is an imaging technique that provides concentrations of trace amounts of compounds labeled with positron-emitting isotopes introduced into the body either by inhalation or intravenous administration [175]. PET techniques have a high sensitivity, such that very low levels of specific tracer accumulation can be detected,

but have an inherently limited spatial resolution [176]. In neuro-oncology the role of PET has been primarily limited to revealing highly specific quantitative information on the metabolic state of gliomas (Fig. 1.14). PET allows the quantitative localization of expression of endogenous or exogenous genes coding for enzymes

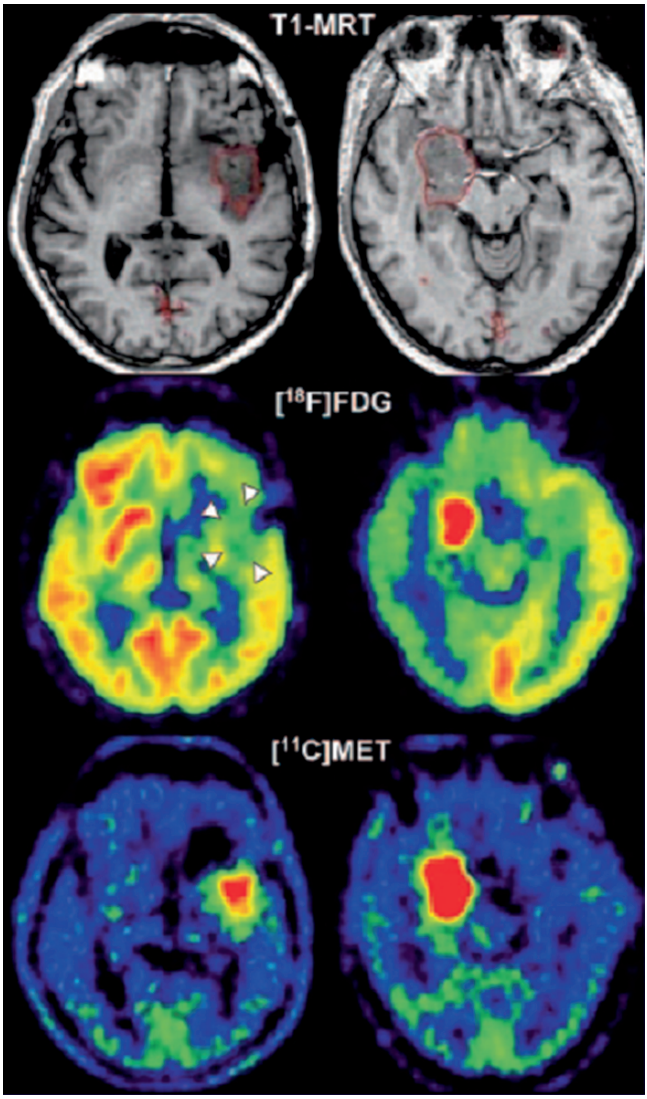

Fig. 1.14 Differentiation between low and high-grade glioma using PET. In low-grade glioma (grade II), glucose metabolism is similar to white matter (arrows) and amino acid uptake is only moderately increased. In high-grade gliomas, both glucose metabolism and amino acid uptake are increased (Printed with permission from Jacobs AH et al., NeuroRX. 2005; 2:333–347.)

or receptors by measuring the accumulation or binding of the respective enzyme substrates or receptor binding compounds [177]. Depending on the radiotracer, various molecular processes can be visualized by PET, most of them relating to an increased cell proliferation within gliomas.

2-[^{18}F] fluoro-2-deoxy-D-glucose (FDG) is the most commonly used tracer for PET oncological studies. FDG's relatively simple synthesis and long half-life, along with extensive knowledge of the mechanisms determining its uptake and retention, have made it quite popular in neuro-oncology [178]. It is well established that brain neoplasms present changes in glucose utilization, compared to normal brain tissue. FDG detects tumor glycolysis and has been used to detect the metabolic differences between normal brain, low-grade and high-grade gliomas [179]. Glucose and FDG share the same saturable carriers between blood and tissue, and FDG competes with glucose for hexokinase. FDG-6-P is trapped in cells in proportion to the glucose metabolic rate, and PET can detect its accumulation. With this tracer, changes in the oxidative metabolism were first demonstrated in vivo in brain neoplasms [180]. Activation of the gene coding for the synthesis of glucose transporter GLUT1 is a major early marker of malignant transformation. An over-expression of GLUT1 and GLUT3 has been observed in brain tumors [181], and this may explain the increased level of glucose extraction demonstrated with PET [182]. The FDG uptake into malignant cells is a consequence of increased expression of glucose transporter and glycolysis. PET-FDG has also been used to differentiate recurrent brain tumors from necrosis after radiation and/or chemotherapy [183]. The areas of necrosis indicate significantly reduced metabolism, while recurrent tumors are identified as having increased metabolism. Kim, et al. [184] evaluated PET imaging in 33 patients with brain tumors after radiation therapy, and found a sensitivity of 80 percent and a specificity of 94 percent for detection of tumor recurrence by FDG-PET.

Oxygen-15 is a short-lived positron-emitting isotope that can be used to measure hemodynamic parameters. Using mathematical modeling, functional images of cerebral blood flow (CBF), oxygen extraction (OER), cerebral oxygen metabolic rate ($CMRO_2$) and blood volume (CBV) can be derived from the combination of sequential studies with $^{15}O_2$, $C^{15}O_2$ and $C^{15}O$. Although blood flow in tumors is variable, oxygen metabolism is generally reduced in gliomas, in line with the relatively anaerobic metabolism of tumors. The low OER implies that the tumor is not ischaemic and that perfusion is sufficient to meet the metabolic need for oxygen in tumors before initiation of therapy [185].

Imaging with radiolabeled amino acids visualizes protein synthesis and amino acid transport phenomena, which are accelerated in tumors [186]. The radiolabeled amino acids methyl- [^{11}C]-L-methionine ([^{11}C] MET), [^{11}C]-tyrosine, [^{18}F] fluoro-tyrosine and O- (2-[^{18}F]-fluoroethyl)-L-tyrosine have been reported to be more specific for brain tumor detection, compared to FDG [187]. [^{11}C] MET-uptake correlates with cell proliferation In Vitro, the expression of Ki-67 and proliferating cell nuclear antigen, as well as to microvessel density, making it a potential biomarker for active tumor proliferation [188]. The intensity of [^{11}C] MET uptake differentiates between grade II and grade III/ IV gliomas [189]. Increased [^{11}C] MET uptake also depends on tumor type, with oligodendrogliomas accumulating more radiotracer

than astrocytomas from the same histological grade [189]. [^{11}C] MET has also been used for guiding stereotactic biopsy of brain tumors [190].

Studies for assessing gene therapy in recurrent gliomas have also been performed. Transduction of the herpes simplex virus type-1 thymidine kinase, followed by subsequent activation of the prodrug ganciclovir, may be beneficial as adjuvant therapy [191]. In future, specific markers of tumor cell proliferation and gene expression may allow the application of PET, not only for diagnostic imaging but also for non-invasive biological characterization of malignant tumors and early monitoring of therapeutic interventions.

5 Key Points

- Neuroimaging of brain tumors has evolved from a purely anatomy-based discipline to one that incorporates morphologic abnormality with physiologic alterations in cellular metabolism and hemodynamics.
- MRI and PET have become an essential part of the diagnostic protocol to diagnose, guide surgery, monitor therapy response and predict prognosis of patients with brain tumors.
- The incorporation of advanced MRI – such as DWI, ^{1}H MRS and PWI – as part of the clinical imaging protocol has empowered neuro-radiologists to begin the process of combining radiology with biology to provide meaningful and clinically relevant end points and biomarkers for clinical trials and assessment of malignancy.
- BOLD-fMRI and diffusion tensor tractography can non-invasively localize the relationship between motor cortex, pyramidal tracts and gliomas to optimize surgical planning with preservation of eloquent areas and subcortical white matters tracts.
- Molecular imaging is a rapidly growing area that should enable evaluation of physiological, biochemical and genetic processes that occur in brain tumors.

References

1. Kleihues P, Soylemezoglu F, Schauble B, Scheithauer BW, Burger PC. Histopathology, classification, and grading of gliomas. Glia 1995; 15:211-221.
2. Daumas-Duport C, Beuvon F, Varlet P, Fallet-Bianco C. [Gliomas: WHO and Sainte-Anne Hospital classifications]. Ann Pathol 2000; 20:413-428.
3. Louis DN, Holland EC, Cairncross JG. Glioma classification: a molecular reappraisal. Am J Pathol 2001; 159:779-786.
4. Furnari FB, Huang HJ, Cavenee WK. Genetics and malignant progression of human brain tumors. Cancer Surv 1995; 25:233-275.
5. Ichimura K, Bolin MB, Goike HM, Schmidt EE, Moshref A, Collins VP. Deregulation of the p14ARF/MDM2/p53 pathway is a prerequisite for human astrocytic gliomas with G1-S transition control gene abnormalities. Cancer Res 2000; 60:417-424.

6. Musicco M, Filippini G, Bordo BM, Melotto A, Morello G, Berrino F. Gliomas and occupational exposure to carcinogens: case-control study. Am J Epidemiol 1982; 116:782-790.
7. Negendank WG, Sauter R, Brown TR, et al. Proton magnetic resonance spectroscopy in patients with glial tumors: a multicenter study. J Neurosurg 1996; 84:449-458.
8. Al-Okaili RN, Krejza J, Wang S, Woo JH, Melhem ER. Advanced MRI Techniques in the Diagnosis of Intra-axial Brain Tumors in Adults. Radiographics 2006; 26 Suppl 1:S173-189.
9. Meyerand ME, Pipas JM, Mamourian A, Tosteson TD, Dunn JF. Classification of biopsy-confirmed brain tumors using single-voxel MR spectroscopy. AJNR Am J Neuroradiol 1999; 20:117-123.
10. Haberg A, Kvistad KA, Unsgard G, Haraldseth O. Preoperative blood oxygen level-dependent functional magnetic resonance imaging in patients with primary brain tumors: clinical application and outcome. Neurosurgery 2004; 54:902-914; discussion 914-905.
11. Pirzkall A, Li X, Oh J, et al. 3D MRSI for resected high-grade gliomas before RT: tumor extent according to metabolic activity in relation to MRI. Int J Radiat Oncol Biol Phys 2004; 59:126-137.
12. Dean BL, Drayer BP, Bird CR, et al. Gliomas: classification with MRI. Radiology 1990; 174:411-415.
13. Atlas SW, Thulborn KR. MR detection of hyperacute parenchymal hemorrhage of the brain. AJNR Am J Neuroradiol 1998; 19:1471-1477.
14. Gupta RK, Rao SB, Jain R, et al. Differentiation of calcification from chronic hemorrhage with corrected gradient echo phase imaging. J Comput Assist Tomogr 2001; 25:698-704.
15. Yamada N, Imakita S, Sakuma T, Takamiya M. Intracranial calcification on gradient-echo phase image: depiction of diamagnetic susceptibility. Radiology 1996; 198:171-178.
16. Atlas SW, Howard RS, 2nd, Maldjian J, et al. Functional magnetic resonance imaging of regional brain activity in patients with intracerebral gliomas: findings and implications for clinical management. Neurosurgery 1996; 38:329-338.
17. Knopp EA, Cha S, Johnson G, et al. Glial neoplasms: dynamic contrast-enhanced T2-weighted MRI. Radiology 1999; 211:791-798.
18. Fayed N, Morales H, Modrego PJ, Pina MA. Contrast/Noise ratio on conventional MRI and choline/creatine ratio on proton MRI spectroscopy accurately discriminate low-grade from high-grade cerebral gliomas. Acad Radiol 2006; 13:728-737.
19. Ricci PE. Imaging of adult brain tumors. Neuroimaging Clin N Am 1999; 9:651-669.
20. Cozad SC, Townsend P, Morantz RA, Jenny AB, Kepes JJ, Smalley SR. Gliomatosis cerebri. Results with radiation therapy. Cancer 1996; 78:1789-1793.
21. White ML, Zhang Y, Smoker WR, et al. Fluid-attenuated inversion-recovery MRI in assessment of intracranial oligodendrogliomas. Comput Med Imaging Graph 2005; 29:279-285.
22. Andreula CF, Recchia-Luciani AN. Rationale for the use of contrast media in MRI. Neuroimaging Clin N Am 1997; 7:461-498.
23. Posner JB, Chernik NL. Intracranial metastases from systemic cancer. Adv Neurol 1978; 19:579-592.
24. Sze G, Milano E, Johnson C, Heier L. Detection of brain metastases: comparison of contrast-enhanced MR with unenhanced MR and enhanced CT. AJNR Am J Neuroradiol 1990; 11:785-791.
25. Yuh WT, Tali ET, Nguyen HD, Simonson TM, Mayr NA, Fisher DJ. The effect of contrast dose, imaging time, and lesion size in the MR detection of intracerebral metastasis. AJNR Am J Neuroradiol 1995; 16:373-380.
26. Sze G, Johnson C, Kawamura Y, et al. Comparison of single- and triple-dose contrast material in the MR screening of brain metastases. AJNR Am J Neuroradiol 1998; 19:821-828.
27. Tang YM, Ngai S, Stuckey S. The solitary enhancing cerebral lesion: can FLAIR aid the differentiation between glioma and metastasis? AJNR Am J Neuroradiol 2006; 27:609-611.
28. Tokumaru A, O'Uchi T, Eguchi T, et al. Prominent meningeal enhancement adjacent to meningioma on Gd-DTPA-enhanced MR images: histopathologic correlation. Radiology 1990; 175:431-433.

29. Nagele T, Petersen D, Klose U, Grodd W, Opitz H, Voigt K. The “dural tail” adjacent to meningiomas studied by dynamic contrast-enhanced MRI: a comparison with histopathology. Neuroradiology 1994; 36:303-307.
30. Kremer P, Forsting M, Hamer J, Sartor K. MR enhancement of the internal auditory canal induced by tissue implant after resection of acoustic neurinoma. AJNR Am J Neuroradiol 1998; 19:115-118.
31. Johnson BA, Fram EK, Johnson PC, Jacobowitz R. The variable MR appearance of primary lymphoma of the central nervous system: comparison with histopathologic features. AJNR Am J Neuroradiol 1997; 18:563-572.
32. Kleihues P, Burger PC, Scheithauer BW. The new WHO classification of brain tumors. Brain Pathol 1993; 3:255-268.
33. Ikushima I, Korogi Y, Hirai T, et al. MR of epidermoids with a variety of pulse sequences. AJNR Am J Neuroradiol 1997; 18:1359-1363.
34. Ernemann U, Rieger J, Tatagiba M, Weller M. An MRI view of a ruptured dermoid cyst. Neurology 2006; 66:270.
35. Plate KH, Risau W. Angiogenesis in malignant gliomas. Glia 1995; 15:339-347.
36. Zagzag D, Zhong H, Scalzitti JM, Laughner E, Simons JW, Semenza GL. Expression of hypoxia-inducible factor 1alpha in brain tumors: association with angiogenesis, invasion, and progression. Cancer 2000; 88:2606-2618.
37. Boxerman JL, Schmainda KM, Weisskoff RM. Relative cerebral blood volume maps corrected for contrast agent extravasation significantly correlate with glioma tumor grade, whereas uncorrected maps do not. AJNR Am J Neuroradiol 2006; 27:859-867.
38. Aronen HJ, Perkio J. Dynamic susceptibility contrast MRI of gliomas. Neuroimaging Clin N Am 2002; 12:501-523.
39. Donahue KM, Krouwer HG, Rand SD, et al. Utility of simultaneously acquired gradient-echo and spin echo cerebral blood volume and morphology maps in brain tumor patients. Magn Reson Med 2000; 43:845-853.
40. Tofts PS, Kermode AG. Measurement of the blood-brain barrier permeability and leakage space using dynamic MRI. 1. Fundamental concepts. Magn Reson Med 1991; 17:357-367.
41. Dixon WT, Du LN, Faul DD, Gado M, Rossnick S. Projection angiograms of blood labeled by adiabatic fast passage. Magn Reson Med 1986; 3:454-462.
42. Sardashti M, Schwartzberg DG, Stomp GP, Dixon WT. Spin-labeling angiography of the carotids by presaturation and simplified adiabatic inversion. Magn Reson Med 1990; 15:192-200.
43. St Lawrence KS, Frank JA, McLaughlin AC. Effect of restricted water exchange on cerebral blood flow values calculated with arterial spin tagging: a theoretical investigation. Magn Reson Med 2000; 44:440-449.
44. Aronen HJ, Gazit IE, Louis DN, et al. Cerebral blood volume maps of gliomas: comparison with tumor grade and histologic findings. Radiology 1994; 191:41-51.
45. Sugahara T, Korogi Y, Kochi M, et al. Correlation of MRI-determined cerebral blood volume maps with histologic and angiographic determination of vascularity of gliomas. AJR Am J Roentgenol 1998; 171:1479-1486.
46. Daumas-Duport C, Tucker ML, Kolles H, et al. Oligodendrogliomas. Part II: A new grading system based on morphological and imaging criteria. J Neurooncol 1997; 34:61-78.
47. Cha S, Tihan T, Crawford F, et al. Differentiation of low-grade oligodendrogliomas from low-grade astrocytomas by using quantitative blood-volume measurements derived from dynamic susceptibility contrast-enhanced MRI. AJNR Am J Neuroradiol 2005; 26:266-273.
48. Gelabert-Gonzalez M, Fernandez-Villa JM, Lopez-Garcia E, Gonzalez-Garcia J, Garcia-Allut A. [Choroid plexus tumors]. Rev Neurol 2001; 33:177-183.
49. Patankar TF, Haroon HA, Mills SJ, et al. Is volume transfer coefficient (K(trans)) related to histologic grade in human gliomas? AJNR Am J Neuroradiol 2005; 26:2455-2465.
50. Pollack IF, Lunsford LD, Flickinger JC, Dameshek HL. Prognostic factors in the diagnosis and treatment of primary central nervous system lymphoma. Cancer 1989; 63:939-947.
51. Cotton F, Ongolo-Zogo P, Louis-Tisserand G, et al. [Diffusion and perfusion MRI in cerebral lymphomas]. J Neuroradiol 2006; 33:220-228.

52. Posner JB. Management of brain metastases. Rev Neurol (Paris) 1992; 148:477-487.
53. Long DM. Capillary ultrastructure in human metastatic brain tumors. J Neurosurg 1979; 51:53-58.
54. Law M, Cha S, Knopp EA, Johnson G, Arnett J, Litt AW. High-grade gliomas and solitary metastases: differentiation by using perfusion and proton spectroscopic MRI. Radiology 2002; 222:715-721.
55. Stewart PA, Hayakawa K, Farrell CL, Del Maestro RF. Quantitative study of microvessel ultrastructure in human peritumoral brain tissue. Evidence for a blood-brain barrier defect. J Neurosurg 1987; 67:697-705.
56. Provenzale JM, Wang GR, Brenner T, Petrella JR, Sorensen AG. Comparison of permeability in high-grade and low-grade brain tumors using dynamic susceptibility contrast MRI. AJR Am J Roentgenol 2002; 178:711-716.
57. Law M, Yang S, Babb JS, et al. Comparison of cerebral blood volume and vascular permeability from dynamic susceptibility contrast-enhanced perfusion MRI with glioma grade. AJNR Am J Neuroradiol 2004; 25:746-755.
58. Roberts HC, Roberts TP, Brasch RC, Dillon WP. Quantitative measurement of microvascular permeability in human brain tumors achieved using dynamic contrast-enhanced MRI: correlation with histologic grade. AJNR Am J Neuroradiol 2000; 21:891-899.
59. George ML, Dzik-Jurasz AS, Padhani AR, et al. Non-invasive methods of assessing angiogenesis and their value in predicting response to treatment in colorectal cancer. Br J Surg 2001; 88:1628-1636.
60. Roberts HC, Roberts TP, Bollen AW, Ley S, Brasch RC, Dillon WP. Correlation of microvascular permeability derived from dynamic contrast-enhanced MRI with histologic grade and tumor labeling index: a study in human brain tumors. Acad Radiol 2001; 8:384-391.
61. Ludemann L, Grieger W, Wurm R, Budzisch M, Hamm B, Zimmer C. Comparison of dynamic contrast-enhanced MRI with WHO tumor grading for gliomas. Eur Radiol 2001; 11:1231-1241.
62. Johnson G, Wetzel SG, Cha S, Babb J, Tofts PS. Measuring blood volume and vascular transfer constant from dynamic, T(2)*-weighted contrast-enhanced MRI. Magn Reson Med 2004; 51:961-968.
63. Wolf RL, Wang J, Wang S, et al. Grading of CNS neoplasms using continuous arterial spin labeled perfusion MRI at 3 Tesla. J Magn Reson Imaging 2005; 22:475-482.
64. Warmuth C, Gunther M, Zimmer C. Quantification of blood flow in brain tumors: comparison of arterial spin labeling and dynamic susceptibility-weighted contrast-enhanced MRI. Radiology 2003; 228:523-532.
65. Chiang IC, Kuo YT, Lu CY, et al. Distinction between high-grade gliomas and solitary metastases using peritumoral 3-T magnetic resonance spectroscopy, diffusion, and perfusion imagings. Neuroradiology 2004; 46:619-627.
66. Burger PC. Morphologic correlates in gliomas: where do we stand? Monogr Pathol 1990:16-29.
67. Muir KW, Buchan A, von Kummer R, Rother J, Baron JC. Imaging of acute stroke. Lancet Neurol 2006; 5:755-768.
68. Bulakbasi N, Kocaoglu M, Ors F, Tayfun C, Ucoz T. Combination of single-voxel proton MR spectroscopy and apparent diffusion coefficient calculation in the evaluation of common brain tumors. AJNR Am J Neuroradiol 2003; 24:225-233.
69. Sundgren PC, Dong Q, Gomez-Hassan D, Mukherji SK, Maly P, Welsh R. Diffusion tensor imaging of the brain: review of clinical applications. Neuroradiology 2004; 46:339-350.
70. Bulakbasi N, Guvenc I, Onguru O, Erdogan E, Tayfun C, Ucoz T. The added value of the apparent diffusion coefficient calculation to magnetic resonance imaging in the differentiation and grading of malignant brain tumors. J Comput Assist Tomogr 2004; 28:735-746.
71. Gupta RK, Sinha U, Cloughesy TF, Alger JR. Inverse correlation between choline magnetic resonance spectroscopy signal intensity and the apparent diffusion coefficient in human glioma. Magn Reson Med 1999; 41:2-7.

72. Sugahara T, Korogi Y, Kochi M, et al. Usefulness of diffusion-weighted MRI with echo-planar technique in the evaluation of cellularity in gliomas. J Magn Reson Imaging 1999; 9:53-60.
73. Kitis O, Altay H, Calli C, Yunten N, Akalin T, Yurtseven T. Minimum apparent diffusion coefficients in the evaluation of brain tumors. Eur J Radiol 2005; 55:393-400.
74. Kono K, Inoue Y, Nakayama K, et al. The role of diffusion-weighted imaging in patients with brain tumors. AJNR Am J Neuroradiol 2001; 22:1081-1088.
75. Yang D, Korogi Y, Sugahara T, et al. Cerebral gliomas: prospective comparison of multivoxel 2D chemical-shift imaging proton MR spectroscopy, echoplanar perfusion and diffusion-weighted MRI. Neuroradiology 2002; 44:656-666.
76. Lam WW, Poon WS, Metreweli C. Diffusion MRI in glioma: does it have any role in the pre-operation determination of grading of glioma? Clin Radiol 2002; 57:219-225.
77. Rollin N, Guyotat J, Streichenberger N, Honnorat J, Tran Minh VA, Cotton F. Clinical relevance of diffusion and perfusion magnetic resonance imaging in assessing intra-axial brain tumors. Neuroradiology 2006; 48:150-159.
78. Fan GG, Deng QL, Wu ZH, Guo QY. Usefulness of diffusion/perfusion-weighted MRI in patients with non-enhancing supratentorial brain gliomas: a valuable tool to predict tumor grading? Br J Radiol 2006; 79:652-658.
79. Lu S, Ahn D, Johnson G, Law M, Zagzag D, Grossman RI. Diffusion-tensor MRI of intracranial neoplasia and associated peritumoral edema: introduction of the tumor infiltration index. Radiology 2004; 232:221-228.
80. Roberts TP, Liu F, Kassner A, Mori S, Guha A. Fiber density index correlates with reduced fractional anisotropy in white matter of patients with glioblastoma. AJNR Am J Neuroradiol 2005; 26:2183-2186.
81. Beppu T, Inoue T, Shibata Y, et al. Fractional anisotropy value by diffusion tensor magnetic resonance imaging as a predictor of cell density and proliferation activity of glioblastomas. Surg Neurol 2005; 63:56-61; discussion 61.
82. Krabbe K, Gideon P, Wagn P, Hansen U, Thomsen C, Madsen F. MR diffusion imaging of human intracranial tumors. Neuroradiology 1997; 39:483-489.
83. Lu S, Ahn D, Johnson G, Cha S. Peritumoral diffusion tensor imaging of high-grade gliomas and metastatic brain tumors. AJNR Am J Neuroradiol 2003; 24:937-941.
84. Yamasaki F, Kurisu K, Satoh K, et al. Apparent diffusion coefficient of human brain tumors at MRI. Radiology 2005; 235:985-991.
85. Guo AC, Cummings TJ, Dash RC, Provenzale JM. Lymphomas and high-grade astrocytomas: comparison of water diffusibility and histologic characteristics. Radiology 2002; 224:177-183.
86. Filippi CG, Edgar MA, Ulug AM, Prowda JC, Heier LA, Zimmerman RD. Appearance of meningiomas on diffusion-weighted images: correlating diffusion constants with histopathologic findings. AJNR Am J Neuroradiol 2001; 22:65-72.
87. Mori S, van Zijl PC. Fiber tracking: principles and strategies - a technical review. NMR Biomed 2002; 15:468-480.
88. Wakana S, Jiang H, Nagae-Poetscher LM, van Zijl PC, Mori S. Fiber tract-based atlas of human white matter anatomy. Radiology 2004; 230:77-87.
89. Catani M, Howard RJ, Pajevic S, Jones DK. Virtual in vivo interactive dissection of white matter fasciculi in the human brain. Neuroimage 2002; 17:77-94.
90. Yu CS, Li KC, Xuan Y, Ji XM, Qin W. Diffusion tensor tractography in patients with cerebral tumors: a helpful technique for neurosurgical planning and postoperative assessment. Eur J Radiol 2005; 56:197-204.
91. Witwer BP, Moftakhar R, Hasan KM, et al. Diffusion-tensor imaging of white matter tracts in patients with cerebral neoplasm. J Neurosurg 2002; 97:568-575.
92. Price SJ, Burnet NG, Donovan T, et al. Diffusion tensor imaging of brain tumors at 3T: a potential tool for assessing white matter tract invasion? Clin Radiol 2003; 58:455-462.
93. Sinha S, Bastin ME, Whittle IR, Wardlaw JM. Diffusion tensor MRI of high-grade cerebral gliomas. AJNR Am J Neuroradiol 2002; 23:520-527.

94. Burlina AP, Aureli T, Bracco F, Conti F, Battistin L. MR spectroscopy: a powerful tool for investigating brain function and neurological diseases. Neurochem Res 2000; 25:1365-1372.
95. Bhakoo KK, Williams IT, Williams SR, Gadian DG, Noble MD. Proton nuclear magnetic resonance spectroscopy of primary cells derived from nervous tissue. J Neurochem 1996; 66:1254-1263.
96. Birken DL, Oldendorf WH. N-acetyl-L-aspartic acid: a literature review of a compound prominent in 1H-NMR spectroscopic studies of brain. Neurosci Biobehav Rev 1989; 13:23-31.
97. Ross B, Michaelis T. Clinical applications of magnetic resonance spectroscopy. Magn Reson Q 1994; 10:191-247.
98. Howe FA, Barton SJ, Cudlip SA, et al. Metabolic profiles of human brain tumors using quantitative in vivo 1H magnetic resonance spectroscopy. Magn Reson Med 2003; 49:223-232.
99. Shimizu H, Kumabe T, Shirane R, Yoshimoto T. Correlation between choline level measured by proton MR spectroscopy and Ki-67 labeling index in gliomas. AJNR Am J Neuroradiol 2000; 21:659-665.
100. Shino A, Nakasu S, Matsuda M, Handa J, Morikawa S, Inubushi T. Noninvasive evaluation of the malignant potential of intracranial meningiomas performed using proton magnetic resonance spectroscopy. J Neurosurg 1999; 91:928-934.
101. Manton DJ, Lowry M, Blackband SJ, Horsman A. Determination of proton metabolite concentrations and relaxation parameters in normal human brain and intracranial tumors. NMR Biomed 1995; 8:104-112.
102. Murphy M, Loosemore A, Clifton AG, et al. The contribution of proton magnetic resonance spectroscopy (1HMRS) to clinical brain tumor diagnosis. Br J Neurosurg 2002; 16:329-334.
103. Ishimaru H, Morikawa M, Iwanaga S, Kaminogo M, Ochi M, Hayashi K. Differentiation between high-grade glioma and metastatic brain tumor using single-voxel proton MR spectroscopy. Eur Radiol 2001; 11:1784-1791.
104. Kreis R, Ernst T, Ross BD. Development of the human brain: In vivo quantification of metabolite and water content with proton magnetic resonance spectroscopy. Magn Reson Med 1993; 30:424-437.
105. Castillo M, Smith JK, Kwock L. Correlation of myo-inositol levels and grading of cerebral astrocytomas. AJNR Am J Neuroradiol 2000; 21:1645-1649.
106. Barba I, Moreno A, Martinez-Perez I, et al. Magnetic resonance spectroscopy of brain hemangiopericytomas: high myoinositol concentrations and discrimination from meningiomas. J Neurosurg 2001; 94:55-60.
107. Norfray JF, Tomita T, Byrd SE, Ross BD, Berger PA, Miller RS. Clinical impact of MR spectroscopy when MRI is indeterminate for pediatric brain tumors. AJR Am J Roentgenol 1999; 173:119-125.
108. Opstad KS, Provencher SW, Bell BA, Griffiths JR, Howe FA. Detection of elevated glutathione in meningiomas by quantitative in vivo 1H MRS. Magn Reson Med 2003; 49:632-637.
109. Stubbs M, Veech RL, Griffiths JR. Tumor metabolism: the lessons of magnetic resonance spectroscopy. Adv Enzyme Regul 1995; 35:101-115.
110. Kugel H, Heindel W, Ernestus RI, Bunke J, du Mesnil R, Friedmann G. Human brain tumors: spectral patterns detected with localized H-1 MR spectroscopy. Radiology 1992; 183:701-709.
111. Alger JR, Frank JA, Bizzi A, et al. Metabolism of human gliomas: assessment with H-1 MR spectroscopy and F-18 fluorodeoxyglucose PET. Radiology 1990; 177:633-641.
112. Auer DP, Gossl C, Schirmer T, Czisch M. Improved analysis of 1H-MR spectra in the presence of mobile lipids. Magn Reson Med 2001; 46:615-618.
113. Kuesel AC, Sutherland GR, Halliday W, Smith IC. 1H MRS of high-grade astrocytomas: mobile lipid accumulation in necrotic tissue. NMR Biomed 1994; 7:149-155.
114. Barba I, Cabanas ME, Arus C. The relationship between nuclear magnetic resonance-visible lipids, lipid droplets, and cell proliferation in cultured C6 cells. Cancer Res 1999; 59:1861-1868.
115. Hakumaki JM, Poptani H, Sandmair AM, Yla-Herttuala S, Kauppinen RA. 1H MRS detects polyunsaturated fatty acid accumulation during gene therapy of glioma: implications for the in vivo detection of apoptosis. Nat Med 1999; 5:1323-1327.

116. Law M, Yang S, Wang H, et al. Glioma grading: sensitivity, specificity, and predictive values of perfusion MRI and proton MR spectroscopic imaging compared with conventional MRI. AJNR Am J Neuroradiol 2003; 24:1989-1998.
117. Herminghaus S, Dierks T, Pilatus U, et al. Determination of histopathological tumor grade in neuroepithelial brain tumors by using spectral pattern analysis of in vivo spectroscopic data. J Neurosurg 2003; 98:74-81.
118. Hsu YY, Chang CN, Wie KJ, Lim KE, Hsu WC, Jung SM. Proton magnetic resonance spectroscopic imaging of cerebral gliomas: correlation of metabolite ratios with histopathologic grading. Chang Gung Med J 2004; 27:399-407.
119. Kaminogo M, Ishimaru H, Morikawa M, et al. Diagnostic potential of short echo time MR spectroscopy of gliomas with single-voxel and point-resolved spatially localised proton spectroscopy of brain. Neuroradiology 2001; 43:353-363.
120. Ott D, Hennig J, Ernst T. Human brain tumors: assessment with in vivo proton MR spectroscopy. Radiology 1993; 186:745-752.
121. Paulus W, Peiffer J. Intratumoral histologic heterogeneity of gliomas. A quantitative study. Cancer 1989; 64:442-447.
122. Cheng LL, Chang IW, Louis DN, Gonzalez RG. Correlation of high-resolution magic angle spinning proton magnetic resonance spectroscopy with histopathology of intact human brain tumor specimens. Cancer Res 1998; 58:1825-1832.
123. Sabatier J, Ibarrola D, Malet-Martino M, Berry I. [Brain tumors: interest of magnetic resonance spectroscopy for the diagnosis and the prognosis]. Rev Neurol (Paris) 2001; 157:858-862.
124. McKnight TR, von dem Bussche MH, Vigneron DB, et al. Histopathological validation of a three-dimensional magnetic resonance spectroscopy index as a predictor of tumor presence. J Neurosurg 2002; 97:794-802.
125. Zhang M, Olsson Y. Hematogenous metastases of the human brain–characteristics of peritumoral brain changes: a review. J Neurooncol 1997; 35:81-89.
126. Fayed N, Modrego PJ. The contribution of magnetic resonance spectroscopy and echoplanar perfusion-weighted MRI in the initial assessment of brain tumors. J Neurooncol 2005; 72:261-265.
127. Beaulieu C, Allen PS. Determinants of anisotropic water diffusion in nerves. Magn Reson Med 1994; 31:394-400.
128. Ogawa S, Menon RS, Tank DW, et al. Functional brain mapping by blood oxygenation level-dependent contrast magnetic resonance imaging. A comparison of signal characteristics with a biophysical model. Biophys J 1993; 64:803-812.
129. Heeger DJ, Ress D. What does fMRI tell us about neuronal activity? Nat Rev Neurosci 2002; 3:142-151.
130. Toronov V, Walker S, Gupta R, et al. The roles of changes in deoxyhemoglobin concentration and regional cerebral blood volume in the fMRI BOLD signal. Neuroimage 2003; 19:1521-1531.
131. Wilkinson ID, Romanowski CA, Jellinek DA, Morris J, Griffiths PD. Motor functional MRI for pre-operative and intraoperative neurosurgical guidance. Br J Radiol 2003; 76:98-103.
132. Pujol J, Conesa G, Deus J, et al. Presurgical identification of the primary sensorimotor cortex by functional magnetic resonance imaging. J Neurosurg 1996; 84:7-13.
133. Pujol J, Conesa G, Deus J, Lopez-Obarrio L, Isamat F, Capdevila A. Clinical application of functional magnetic resonance imaging in presurgical identification of the central sulcus. J Neurosurg 1998; 88:863-869.
134. Lehericy S, Duffau H, Cornu P, et al. Correspondence between functional magnetic resonance imaging somatotopy and individual brain anatomy of the central region: comparison with intraoperative stimulation in patients with brain tumors. J Neurosurg 2000; 92:589-598.
135. Lee CC, Ward HA, Sharbrough FW, et al. Assessment of functional MRI in neurosurgical planning. AJNR Am J Neuroradiol 1999; 20:1511-1519.
136. Fandino J, Kollias SS, Wieser HG, Valavanis A, Yonekawa Y. Intraoperative validation of functional magnetic resonance imaging and cortical reorganization patterns in patients with brain tumors involving the primary motor cortex. J Neurosurg 1999; 91:238-250.

137. Holodny AI, Schulder M, Liu WC, Wolko J, Maldjian JA, Kalnin AJ. The effect of brain tumors on BOLD functional MRI activation in the adjacent motor cortex: implications for image-guided neurosurgery. AJNR Am J Neuroradiol 2000; 21:1415-1422.
138. Ulmer JL, Hacein-Bey L, Mathews VP, et al. Lesion-induced pseudo-dominance at functional magnetic resonance imaging: implications for preoperative assessments. Neurosurgery 2004; 55:569-579; discussion 580-561.
139. Schreiber A, Hubbe U, Ziyeh S, Hennig J. The influence of gliomas and nonglial space-occupying lesions on blood-oxygen-level-dependent contrast enhancement. AJNR Am J Neuroradiol 2000; 21:1055-1063.
140. Hossmann KA, Linn F, Okada Y. Bioluminescence and fluoroscopic imaging of tissue pH and metabolites in experimental brain tumors of cat. NMR Biomed 1992; 5:259-264.
141. Laurienti PJ, Field AS, Burdette JH, Maldjian JA, Yen YF, Moody DM. Dietary caffeine consumption modulates fMRI measures. Neuroimage 2002; 17:751-757.
142. Buhmann C, Glauche V, Sturenburg HJ, Oechsner M, Weiller C, Buchel C. Pharmacologically modulated fMRI–cortical responsiveness to levodopa in drug-naive hemiparkinsonian patients. Brain 2003; 126:451-461.
143. Kamada K, Todo T, Masutani Y, et al. Combined use of tractography-integrated functional neuronavigation and direct fiber stimulation. J Neurosurg 2005; 102:664-672.
144. Li ZX, Dai JP, Jiang T, et al. [Function magnetic resonance imaging and diffusion tensor tractography in patients with brain gliomas involving motor areas: clinical application and outcome]. Zhonghua Wai Ke Za Zhi 2006; 44:1275-1279.
145. Schonberg T, Pianka P, Hendler T, Pasternak O, Assaf Y. Characterization of displaced white matter by brain tumors using combined DTI and fMRI. Neuroimage 2006; 30:1100-1111.
146. Bonavita S, Di Salle F, Tedeschi G. Proton MRS in neurological disorders. Eur J Radiol 1999; 30:125-131.
147. Burger PC, Fuller GN. Pathology–trends and pitfalls in histologic diagnosis, immunopathology, and applications of oncogene research. Neurol Clin 1991; 9:249-271.
148. Fulham MJ, Bizzi A, Dietz MJ, et al. Mapping of brain tumor metabolites with proton MR spectroscopic imaging: clinical relevance. Radiology 1992; 185:675-686.
149. Sijens PE, Vecht CJ, Levendag PC, van Dijk P, Oudkerk M. Hydrogen magnetic resonance spectroscopy follow-up after radiation therapy of human brain cancer. Unexpected inverse correlation between the changes in tumor choline level and post-gadolinium magnetic resonance imaging contrast. Invest Radiol 1995; 30:738-744.
150. Usenius T, Usenius JP, Tenhunen M, et al. Radiation-induced changes in human brain metabolites as studied by 1H nuclear magnetic resonance spectroscopy in vivo. Int J Radiat Oncol Biol Phys 1995; 33:719-724.
151. Taylor JS, Langston JW, Reddick WE, et al. Clinical value of proton magnetic resonance spectroscopy for differentiating recurrent or residual brain tumor from delayed cerebral necrosis. Int J Radiat Oncol Biol Phys 1996; 36:1251-1261.
152. Sugahara T, Korogi Y, Tomiguchi S, et al. Posttherapeutic intraaxial brain tumor: the value of perfusion-sensitive contrast-enhanced MRI for differentiating tumor recurrence from non-neoplastic contrast-enhancing tissue. AJNR Am J Neuroradiol 2000; 21:901-909.
153. Hein PA, Eskey CJ, Dunn JF, Hug EB. Diffusion-weighted imaging in the follow-up of treated high-grade gliomas: tumor recurrence versus radiation injury. AJNR Am J Neuroradiol 2004; 25:201-209.
154. Asao C, Korogi Y, Kitajima M, et al. Diffusion-weighted imaging of radiation-induced brain injury for differentiation from tumor recurrence. AJNR Am J Neuroradiol 2005; 26:1455-1460.
155. Willems JG, Alva-Willems JM. Accuracy of cytologic diagnosis of central nervous system neoplasms in sterotactic biopsies. Acta Cytol 1984; 28:243-249.
156. Fratkin JD, Ward MM, Roberts DW, Sullivan MM. CT-guided stereotactic biopsy of intracranial lesions: correlation between core biopsy and aspiration smear. Diagn Cytopathol 1986; 2:126-132.
157. Krieger MD, Chandrasoma PT, Zee CS, Apuzzo ML. Role of stereotactic biopsy in the diagnosis and management of brain tumors. Semin Surg Oncol 1998; 14:13-25.

158. Kelly PJ, Daumas-Duport C, Kispert DB, Kall BA, Scheithauer BW, Illig JJ. Imaging-based stereotaxic serial biopsies in untreated intracranial glial neoplasms. J Neurosurg 1987; 66:865-874.
159. Cha S, Knopp EA, Johnson G, Wetzel SG, Litt AW, Zagzag D. Intracranial mass lesions: dynamic contrast-enhanced susceptibility-weighted echo-planar perfusion MRI. Radiology 2002; 223:11-29.
160. Baik HM, Choe BY, Son BC, et al. Feasibility of proton chemical shift imaging with a stereotactic headframe. Magn Reson Imaging 2003; 21:55-59.
161. Kondziolka D, Somaza S, Comey C, et al. Radiosurgery and fractionated radiation therapy: comparison of different techniques in an in vivo rat glioma model. J Neurosurg 1996; 84:1033-1038.
162. Hormigo A, Friedlander DR, Brittis PA, Zagzag D, Grumet M. Reduced tumorigenicity of rat glioma cells in the brain when mediated by hygromycin phosphotransferase. J Neurosurg 2001; 94:596-604.
163. Hakumaki JM, Poptani H, Puumalainen AM, et al. Quantitative 1H nuclear magnetic resonance diffusion spectroscopy of BT4C rat glioma during thymidine kinase-mediated gene therapy in vivo: identification of apoptotic response. Cancer Res 1998; 58:3791-3799.
164. Jacobs AH, Dittmar C, Winkeler A, Garlip G, Heiss WD. Molecular imaging of gliomas. Mol Imaging 2002; 1:309-335.
165. Zhang Z, Jiang Q, Jiang F, et al. in vivo magnetic resonance imaging tracks adult neural progenitor cell targeting of brain tumor. Neuroimage 2004; 23:281-287.
166. Magnitsky S, Watson DJ, Walton RM, et al. in vivo and Ex Vivo MRI detection of localized and disseminated neural stem cell grafts in the mouse brain. Neuroimage 2005; 26:744-754.
167. Su H, Forbes A, Gambhir SS, Braun J. Quantitation of cell number by a positron emission tomography reporter gene strategy. Mol Imaging Biol 2004; 6:139-148.
168. Doubrovin M, Ponomarev V, Beresten T, et al. Imaging transcriptional regulation of p53-dependent genes with positron emission tomography in vivo. Proc Natl Acad Sci U S A 2001; 98:9300-9305.
169. Serganova I, Doubrovin M, Vider J, et al. Molecular imaging of temporal dynamics and spatial heterogeneity of hypoxia-inducible factor-1 signal transduction activity in tumors in living mice. Cancer Res 2004; 64:6101-6108.
170. Uhrbom L, Nerio E, Holland EC. Dissecting tumor maintenance requirements using bioluminescence imaging of cell proliferation in a mouse glioma model. Nat Med 2004; 10:1257-1260.
171. Wen B, Burgman P, Zanzonico P, et al. A preclinical model for noninvasive imaging of hypoxia-induced gene expression; comparison with an exogenous marker of tumor hypoxia. Eur J Nucl Med Mol Imaging 2004; 31:1530-1538.
172. Gillies RJ, Raghunand N, Karczmar GS, Bhujwalla ZM. MRI of the tumor microenvironment. J Magn Reson Imaging 2002; 16:430-450.
173. Garcia-Martin ML, Martinez GV, Raghunand N, Sherry AD, Zhang S, Gillies RJ. High resolution pH(e) imaging of rat glioma using pH-dependent relaxivity. Magn Reson Med 2006; 55:309-315.
174. Poptani H, Duvvuri U, Miller CG, et al. T1rho imaging of murine brain tumors at 4 T. Acad Radiol 2001; 8:42-47.
175. Phelps ME, Mazziotta JC. Positron emission tomography: human brain function and biochemistry. Science 1985; 228:799-809.
176. Phelps ME. PET: the merging of biology and imaging into molecular imaging. J Nucl Med 2000; 41:661-681.
177. Price P. PET as a potential tool for imaging molecular mechanisms of oncology in man. Trends Mol Med 2001; 7:442-446.

178. Heiss WD, Heindel W, Herholz K, et al. Positron emission tomography of fluorine-18-deoxyglucose and image-guided phosphorus-31 magnetic resonance spectroscopy in brain tumors. J Nucl Med 1990; 31:302-310.
179. Herholz K, Heindel W, Luyten PR, et al. in vivo imaging of glucose consumption and lactate concentration in human gliomas. Ann Neurol 1992; 31:319-327.
180. Mineura K, Yasuda T, Kowada M, Shishido F, Ogawa T, Uemura K. Positron emission tomographic evaluation of histological malignancy in gliomas using oxygen-15 and fluorine-18-fluorodeoxyglucose. Neurol Res 1986; 8:164-168.
181. Nishioka T, Oda Y, Seino Y, et al. Distribution of the glucose transporters in human brain tumors. Cancer Res 1992; 52:3972-3979.
182. Brooks DJ, Beaney RP, Lammertsma AA, et al. Glucose transport across the blood-brain barrier in normal human subjects and patients with cerebral tumors studied using [11C]3-O-methyl-D-glucose and positron emission tomography. J Cereb Blood Flow Metab 1986; 6:230-239.
183. Glantz MJ, Hoffman JM, Coleman RE, et al. Identification of early recurrence of primary central nervous system tumors by [18F]fluorodeoxyglucose positron emission tomography. Ann Neurol 1991; 29:347-355.
184. Kim EE, Chung SK, Haynie TP, et al. Differentiation of residual or recurrent tumors from post-treatment changes with F-18 FDG PET. Radiographics 1992; 12:269-279.
185. Tyler JL, Diksic M, Villemure JG, et al. Metabolic and hemodynamic evaluation of gliomas using positron emission tomography. J Nucl Med 1987; 28:1123-1133.
186. Isselbacher KJ. Sugar and amino acid transport by cells in culture–differences between normal and malignant cells. N Engl J Med 1972; 286:929-933.
187. Jager PL, Vaalburg W, Pruim J, de Vries EG, Langen KJ, Piers DA. Radiolabeled amino acids: basic aspects and clinical applications in oncology. J Nucl Med 2001; 42:432-445.
188. Sato N, Suzuki M, Kuwata N, et al. Evaluation of the malignancy of glioma using 11C-methionine positron emission tomography and proliferating cell nuclear antigen staining. Neurosurg Rev 1999; 22:210-214.
189. Herholz K, Holzer T, Bauer B, et al. 11C-methionine PET for differential diagnosis of low-grade gliomas. Neurology 1998; 50:1316-1322.
190. Goldman S, Levivier M, Pirotte B, et al. Regional methionine and glucose uptake in high-grade gliomas: a comparative study on PET-guided stereotactic biopsy. J Nucl Med 1997; 38:1459-1462.
191. Jacobs A, Tjuvajev JG, Dubrovin M, et al. Positron emission tomography-based imaging of transgene expression mediated by replication-conditional, oncolytic herpes simplex virus type 1 mutant vectors in vivo. Cancer Res 2001; 61:2983-2995.